



UNIVERSIDAD DE INVESTIGACIÓN DE TECNOLOGÍA EXPERIMENTAL YACHAY

Escuela de Ciencias Matemáticas y Computacionales

TÍTULO: Comparison of radial distortion correction models for self photogrammetric camera calibration

Trabajo de integración curricular presentado como requisito para
la obtención del título de Ingeniero en Tecnologías de la
Información

Autor:

Molina Ron María Fernanda

Tutor:

Antón Castro Francesc, PhD

Urququí, julio de 2020

SECRETARÍA GENERAL
(Vicerrectorado Académico/Cancillería)
ESCUELA DE CIENCIAS MATEMÁTICAS Y COMPUTACIONALES
CARRERA DE TECNOLOGÍAS DE LA INFORMACIÓN
ACTA DE DEFENSA No. UITEY-ITE-2020-00026-AD

A los 21 días del mes de julio de 2020, a las 11:00 horas, de manera virtual mediante videoconferencia, y ante el Tribunal Calificador, integrado por los docentes:

Presidente Tribunal de Defensa	Dr. MAYORGA ZAMBRANO, JUAN RICARDO , Ph.D.
Miembro No Tutor	Dr. ARIZA GARCIA, EUSEBIO ALBERTO , Ph.D.
Tutor	Dr. ANTÓN CASTRO , FRANCESC , Ph.D.

El(la) señor(ita) estudiante **MOLINA RON, MARIA FERNANDA**, con cédula de identidad No. **1718515545**, de la **ESCUELA DE CIENCIAS MATEMÁTICAS Y COMPUTACIONALES**, de la Carrera de **TECNOLOGÍAS DE LA INFORMACIÓN**, aprobada por el Consejo de Educación Superior (CES), mediante Resolución **RPC-SO-43-No.496-2014**, realiza a través de videoconferencia, la sustentación de su trabajo de titulación denominado: **COMPARISON OF RADIAL DISTORTION CORRECTION MODELS FOR SELF PHOTOGRAMMETRIC CAMERA CALIBRATION**, previa a la obtención del título de **INGENIERO/A EN TECNOLOGÍAS DE LA INFORMACIÓN**.

El citado trabajo de titulación, fue debidamente aprobado por el(los) docente(s):

Tutor	Dr. ANTÓN CASTRO , FRANCESC , Ph.D.
--------------	-------------------------------------

Y recibió las observaciones de los otros miembros del Tribunal Calificador, las mismas que han sido incorporadas por el(la) estudiante.

Previamente cumplidos los requisitos legales y reglamentarios, el trabajo de titulación fue sustentado por el(la) estudiante y examinado por los miembros del Tribunal Calificador. Escuchada la sustentación del trabajo de titulación a través de videoconferencia, que integró la exposición de el(la) estudiante sobre el contenido de la misma y las preguntas formuladas por los miembros del Tribunal, se califica la sustentación del trabajo de titulación con las siguientes calificaciones:

Tipo	Docente	Calificación
Presidente Tribunal De Defensa	Dr. MAYORGA ZAMBRANO, JUAN RICARDO , Ph.D.	10,0
Tutor	Dr. ANTÓN CASTRO , FRANCESC , Ph.D.	10,0
Miembro Tribunal De Defensa	Dr. ARIZA GARCIA, EUSEBIO ALBERTO , Ph.D.	10,0

Lo que da un promedio de: **10 (Diez punto Cero)**, sobre 10 (diez), equivalente a: **APROBADO**

Para constancia de lo actuado, firman los miembros del Tribunal Calificador, el/la estudiante y el/la secretario ad-hoc.

MOLINA RON, MARIA FERNANDA
Estudiante

Dr. MAYORGA ZAMBRANO, JUAN RICARDO , Ph.D.
Presidente Tribunal de Defensa



Firmado electrónicamente por:
JUAN RICARDO
MAYORGA
ZAMBRANO

Dr. ANTÓN CASTRO , FRANCESC , Ph.D.
Tutor

FRANCE
SC
ANTON
CASTRO

Signé électroniquement par
FRANCESCO ANTON CASTRO
c=FRANCESCO ANTON CASTRO,
o=ENTIDAD DE CERTIFICACION
DE INFORMACION, s=SECURITY
DATA S.A. 1, c=EC
Date: 2020.07.21 11:40:53 ECT

Dr. ARIZA GARCIA, EUSEBIO ALBERTO , Ph.D.
Miembro No Tutor

EUSEBIO ALBERTO
ARIZA GARCIA

Firmado digitalmente por
EUSEBIO ALBERTO ARIZA GARCIA
Fecha: 2020.07.21 11:48:11
-05'00'

MEDINA BRITO, DAYSY MARGARITA
Secretario Ad-hoc

DAYSY MARGARITA
MEDINA BRITO

Firmado digitalmente por DAYSY
MARGARITA MEDINA BRITO
Fecha: 2020.07.21 11:56:16 -05'00'

Autoría

Yo, **MARÍA FERNANDA MOLINA RON**, con cédula de identidad 1718515545, declaro que las ideas, juicios, valoraciones, interpretaciones, consultas bibliográficas, definiciones y conceptualizaciones expuestas en el presente trabajo; así cómo, los procedimientos y herramientas utilizadas en la investigación, son de absoluta responsabilidad de el/la autor(a) del trabajo de integración curricular. Así mismo, me acojo a los reglamentos internos de la Universidad de Investigación de Tecnología Experimental Yachay.

Urququí, julio del 2020.



María Fernanda Molina Ron

CI: 1718515545

Autorización de publicación

Yo, **MARÍA FERNANDA MOLINA RON**, con cédula de identidad 1718515545, cedo a la Universidad de Tecnología Experimental Yachay, los derechos de publicación de la presente obra, sin que deba haber un reconocimiento económico por este concepto. Declaro además que el texto del presente trabajo de titulación no podrá ser cedido a ninguna empresa editorial para su publicación u otros fines, sin contar previamente con la autorización escrita de la Universidad.

Asimismo, autorizo a la Universidad que realice la digitalización y publicación de este trabajo de integración curricular en el repositorio virtual, de conformidad a lo dispuesto en el Art. 144 de la Ley Orgánica de Educación Superior.

Urcuquí, julio del 2020.



María Fernanda Molina Ron

CI: 1718515545

Dedication

“In dedication to my mother, Verónica Ron, a strong and patient woman. I would not be the person I am today without her love and sacrifices. To my father, Xavier Molina, for his advice, guidance and motivation during my whole career and through this research. Both have always been my complete inspiration that make me able to reach this challenge with success and honor.”

María Fernanda Molina Ron

Acknowledgements

“I would like to express my sincere gratitude to my dedicated advisor Francesc Antón Castro who gave me the opportunity and support to do this research, for his patience, advise and knowledge. I am also extremely grateful to my parents and family for being the best support team during my whole career.

Thanks also to all the people who make part of Yachay Tech University. I appreciate being part of this educational project. Each of their professors and professionals have contributed and inspired me at this stage of my life. I would like to thank two professionals in particular who accompanied me during my personal and emotional growth process, Psych. Verónica Carchipulla and Psych. Andres Borja.

Finally, my life at university would not be such an incredible experience and full of good memories without all the friends I have made. They have been my support and joy during all my time away from home and through the different challenges that the university has brought to me. There are several, but I will do my best to not omit anyone. Thanks to: Bernardo, Marlon, Pablo, Osiris, Emil, Saulo, Alex, Sebas, Antoni, Jorge, Sergio, Giss, Yachay’s soccer team, Cristhian, Luis, Bryan, Demetrio and Isaac. Thanks to my childhood girlfriends: Mishell, Jahel, Pao G., Pame and Pao V. I wish you all success in your personal and professional life.”

María Fernanda Molina Ron

Resumen

En muchos campos, como la visión computacional, la robótica y la fotogrametría, el uso de cámaras es muy importante para ejecutar diferentes tareas. Para lograr esas tareas con éxito, es necesario llevar a cabo una calibración de las cámaras como un paso esencial antes de ejecutar dichas tareas. En fotogrametría, la fiabilidad de la calibración de la cámara es esencial para realizar mediciones decisivas. Las distorsiones de la lente de la cámara tienen un impacto significativo en la geometría de la imagen y, en consecuencia, en la calibración de la cámara en general. El problema abordado en esta tesis es la calibración confiable de la distorsión radial de las cámaras, que es indispensable para poder realizar mediciones confiables. Esta tesis compara las aplicaciones de diferentes métodos algebraicos y sus modelos de la distorsión radial de manera totalmente determinista utilizando solo 2 ortofotografías de un cubo personalizado con un patrón reticular. Como resultados notables, se demuestra experimentalmente que los modelos obtenidos con los métodos que minimizan la distancia Ortogonal y Vertical siempre dan los mejores resultados para casi todos los experimentos. Además, el método de Wu es el mejor método de interpolación para un pequeño conjunto de datos de puntos característicos. Además, Cubic Spline Interpolation tiene muy poco control sobre los picos, lo que produce resultados no muy óptimos con conjuntos de datos más grandes para algunos experimentos. Finalmente, el clustering ayuda a reducir el conjunto de datos de puntos característicos y también produce buenos modelos de corrección de distorsión radial.

Keywords: Fotogrametría, Calibración de cámara, distorsión radial del lente, métodos algebraicos, algoritmos deterministas, ortofotos.

Abstract

In many fields such as computational vision, robotics and photogrammetry, the use of cameras is very important in order to execute different tasks. In order to achieve those tasks successfully, it is necessary to carry out a calibration of the cameras as an essential step before any of them. In photogrammetry, the reliability of camera calibration is essential to take decisive measurements. Camera lens distortions have a significant impact on image geometry and consequently, on camera calibration in general. The problem addressed in this thesis is the reliable radial distortion calibration of cameras, which is indispensable for being able to perform reliable measurements. This thesis compares the applications of different algebraic methods and their obtained models to the fully deterministic radial distortion correction only using 2 orthophotographs of a personalized cube with a lattice pattern on it into. As remarkable results, it is experimentally proved that models obtained with the methods that minimizes the Orthogonal and Vertical distance always give best results for almost all the experiments. In addition, Wu's method is the best interpolation method for a small feature point data set. Also, Cubic Spline has a little control over spikes which produces not very good results with bigger data sets for some experiments. Finally, clustering helps to reduce the feature points data set and also produces good radial distortion correction models.

Keywords: Photogrammetry, Camera Calibration, radial lens distortion, algebraic methods, deterministic algorithms, orthophotographs.

Contents

Introduction	9
1 Preliminaries	11
1.1 Problem statement	11
1.2 Justification and Contribution	15
1.3 Objectives	15
1.3.1 General Objective	15
1.3.2 Specific Objectives	16
1.4 Document organization	16
2 Theoretical Framework	17
2.1 Pinhole Camera Model	17
2.2 The Lens System	18
2.3 Mathematical Model	21
2.4 Data Fitting Algebraic Methods	21
2.4.1 Minimize the sum of squares of the vertical distance	21
2.4.2 Minimize the sum of squares of the orthogonal distance	24
2.4.3 Cubic Spline Interpolation	26
2.4.4 Wu's polynomial elimination	34
2.4.5 Legendre Polynomials Approximation	35
2.5 Error Measure	36
2.5.1 Root Mean Square Error	36
2.5.2 L-infinity Norm	36

3	Methodology	37
3.1	Lattice	37
3.2	Orthophoto	38
3.3	Feature Points Detection	40
3.4	Radial Distortion	41
3.5	Experiments	43
3.5.1	Experiment 1: 81 Feature Points	43
3.5.2	Experiment 2: 5 Greatest Feature Points in Distortion	49
3.5.3	Experiment 3: Clusters	54
3.5.4	Experiment 4: Residuals of the 81 Feature Points and all the models	57
4	Results and Discussion	60
4.1	Experiment 1: 81 Feature Points	60
4.1.1	Orthophoto 1:	61
4.1.2	Orthophoto 2	62
4.2	Experiment 2: 5 Greatest Distortion Feature Points	63
4.2.1	Orthophoto 1:	64
4.2.2	Orthophoto 2	65
4.3	Experiment 3: Clusters	67
4.3.1	Orthophoto 1	68
4.3.2	Orthophoto 2	69
4.4	Experiment 4: 81 Feature Points VS all the models	70
4.4.1	Orthophoto 1 - Models obtained with 5 observations VS 81 obser- vations	71
4.4.2	Orthophoto 2 - Models obtained with 5 observations VS 81 obser- vations	73
4.4.3	Orthophoto 1 -Models obtained with 55 centroids VS 81 observations	75
4.4.4	Orthophoto 2 - Models obtained with 55 centroids VS 81 observations	78
5	Conclusions and future work	80

References	83
Appendices	87
A Extra Definitions	88
A.1 Rings	88
A.2 Ideals	89
A.3 Rings of Polynomials	89
A.4 Division Algorithm for Polynomials	90
A.5 Wu's Method	90

List of Figures

- 1.1 A classical example of aerial photogrammetric camera photograph. *Source:* [1] 12
- 1.2 The difference between the perspective projection of normal photographs and the orthogonal projection of orthophotographs 13
- 1.3 First pages of a Zeiss calibration report from Denmark’s Kort og Matrikel Styrelsen 14
- 1.4 Last pages of the same Zeiss calibration report from Denmark’s Kort og Matrikel Styrelsen 14

- 2.1 Projection center and image plane. *Source:* [2] 17
- 2.2 Pinhole Camera Geometry. *Source:* [2] 18
- 2.3 Lens System. *Source:* [2] 19
- 2.4 Radial and Tangential Distortion. *Source:* [3] 20
- 2.5 Orthogonal distance vs Vertical Distance 26

- 3.1 Lattice pattern image produced by GeoGebra. 37
- 3.2 Orthophoto 1 39
- 3.3 Orthophoto 2 39
- 3.4 Manual Feature Points Detection using GIMP 41
- 3.5 Lattice pattern image superimposed on Orthophoto 1 42
- 3.6 Lattice pattern image superimposed on Orthophoto 2 43
- 3.7 Orthogonal distance vs Vertical Distance 48

4.1	Calibration model obtained with VDM and ODM	61
4.2	Calibration model obtained with VDM and ODM	62
4.3	Calibration model obtained with VDM and ODM	64
4.4	Calibration model obtained with Cubic Spline Method	65
4.5	Calibration model obtained with Wu's Method	65
4.6	Calibration model obtained with VDM and ODM	66
4.7	Calibration model obtained with Cubic Spline Method	66
4.8	Calibration model obtained with Wu's Method	67
4.9	Calibration model obtained with VDM and ODM	68
4.10	Calibration model obtained with Cubic Spline Method	68
4.11	Calibration model obtained with VDM and ODM	69
4.12	Calibration model obtained with Cubic Spline Method	70
4.13	Calibration model obtained with 5 points with VDM and ODM VS 81 feature points	72
4.14	Calibration model obtained with 5 points with Cubic Spline VS 81 feature points	72
4.15	Calibration model obtained with 5 points with Wu VS 81 feature points . .	73
4.16	Calibration model obtained with 5 points with VDM and ODM VS 81 feature points	74
4.17	Calibration model obtained with 5 points with Cubic Spline VS 81 feature points	75
4.18	Calibration model obtained with 5 points with Wu VS 81 feature points . .	75
4.19	Calibration model obtained with 55 centroids with VDM and ODM VS 81 feature points	76
4.20	Calibration model obtained with 55 centroids with Cubic Spline VS 81 feature points	77
4.21	Calibration model obtained with 55 centroids with VDM and ODM VS 81 feature points	78

4.22 Calibration model obtained with 55 centroids with Cubic Spline VS 81
feature points 78

List of Tables

4.1	Experiment 1 - Comparison of Root Square Mean Error and L-infinity Norm of each model	61
4.2	Experiment 1 - Comparison of Root Square Mean Error and L-infinity Norm of each model in pixels	62
4.3	Experiment 1 - Comparison of Root Square Mean Error and L-infinity Norm of each model	62
4.4	Experiment 1 - Comparison of Root Square Mean Error and L-infinity Norm of each model in pixels	63
4.5	Experiment 2 : 5 Greatest Feature Points in Distortion - Comparison of Root Square Mean Error and L-infinity Norm.	64
4.6	Experiment 2 : 5 Greatest Feature Points in Distortion - Comparison of Root Square Mean Error and L-infinity Norm in pixels	64
4.7	Experiment 2 : 5 Greatest in Distortion Feature Points - Comparison of Root Square Mean Error and L-infinity Norm.	65
4.8	Experiment 2 : 5 Greatest in Distortion Feature Points - Comparison of Root Square Mean Error and L-infinity Norm in pixels	66
4.9	Experiment 3 : Cluster - Comparison of Root Square Mean Error and L-infinity Norm.	69
4.10	Experiment 3 : Cluster - Comparison of Root Square Mean Error and L-infinity Norm in pixels.	69
4.11	Experiment 3 : Cluster - Comparison of Root Square Mean Error and L-infinity Norm.	70

4.12 Experiment 3 : Cluster - Comparison of Root Square Mean Error and L-infinity Norm in pixels. 70

4.13 Experiment 4 : 81 Feature Points VS the models with 5 points - Comparison of Root Square Mean Error and L-infinity Norm. 71

4.14 Experiment 4 : 81 Feature Points VS the models with 5 points - Comparison of Root Square Mean Error and L-infinity Norm in pixels. 72

4.15 Experiment 4 : 81 Feature Points VS the models with 5 points - Comparison of Root Square Mean Error and L-infinity Norm. 74

4.16 Experiment 4 : 81 Feature Points VS the models with 5 points - Comparison of Root Square Mean Error and L-infinity Norm in pixels. 74

4.17 Experiment 4 : 81 Feature Points VS the models with 55 centroids - Comparison of Root Square Mean Error and L-infinity Norm. 77

4.18 Experiment 4 : 81 Feature Points VS the models with 55 centroids - Comparison of Root Square Mean Error and L-infinity Norm in pixels. 77

4.19 Experiment 4 : 81 Feature Points VS the models with 55 centroids - Comparison of Root Square Mean Error and L-infinity Norm. 79

4.20 Experiment 4 : 81 Feature Points VS the models with 55 centroids - Comparison of Root Square Mean Error and L-infinity Norm in pixels. 79

Introduction

Within many fields such as computational vision, robotics and photogrammetry, the use of cameras is very important for different tasks like: detection and measurement of objects, navigation systems, topographic mapping, reconstruction of three-dimensional scenes, and many others. For these tasks to be executed successfully, it is necessary to carry out a calibration of the cameras before.

Camera Calibration is an important component of any vision task used to determine the mapping relationship between the 3D world and its corresponding 2D image. So far, a variety of calibration methods [4], have been developed to adapt to different applications and deal with almost all problems of camera calibration. In photogrammetry, the reliability of camera calibration is essential to take decisive measurements. Current photogrammetric software uses non-deterministic algorithms to perform the camera calibration. Non-deterministic algorithms can produce different outputs on various executions, even for the same input. Thus, these algorithms do not give reliable metric information from images.

For most photogrammetric applications, it is common to use the projective pinhole camera model to determine the intrinsic and extrinsic parameters of the camera, but this model does not take into account the camera lens distortion. Camera lens distortions have a significant impact on image geometry and consequently on camera calibration in general. Lens distortion is principally radial and therefore, camera models can be augmented with a radial lens distortion model to compensate for lens distortion effects and improve

the camera model. This means that the calibration camera procedure can estimate the parameters of the lens distortion model together with the rest of camera calibration parameters or they can be calculated separately, [5] and [6] .

In this context, this thesis presents a fully deterministic distortion correction with an analysis and comparison of the performance of models obtained with different algebraic data fitting methods using only 2 orthophotographs of a personalized cube with a lattice pattern on it.

Chapter 1

Preliminaries

1.1 Problem statement

The realm of the problem addressed in this thesis is Photogrammetry. Photogrammetry is “*the art, science and technology of obtaining reliable information about physical objects and the environment through the process of recording, measuring and interpreting photographic images and patterns of electromagnetic radiant imagery and other phenomena*”[7].

The problem addressed in this thesis is the reliable calibration of cameras, which is indispensable for being able to perform reliable measurements. Current photogrammetric software suites, independently from their commercial or open source nature, have incorporated algorithms from Computer Vision, which are not deterministic, such as the Scale-Invariant Feature Transform (SIFT) [8], or the Speeded up Robust Features (SURF) [9] algorithms.

Non-determinism is not acceptable for the Photogrammeter, who wants to obtain reliable metric information from images, whether they are photographs, optical, radar, hyperspectral or multispectral satellite images, echographies, multi-beam echo sounder images, computer tomographies or any other image, i.e., one or several mappings from \mathbb{R}^n to \mathbb{R} (each layer corresponding to such a mapping), since the Photogrammeter cannot accept that an algorithm will give different results on the same input images. This determinism requirement is very important as photogrammetric surveys are used in order

to take life-critical decisions, like building a bridge, a dam, an arrangement of surgical equipments, etc.

This thesis addresses the problem of non-determinism of the feature detection in photogrammetric suites in the context of photogrammetric calibration of cameras. The main objective of the calibration of a camera is the production of a calibration report (see an example in Figures 1.3 and 1.4), that will be used to correct the images taken with the camera, object of the calibration.

In the old photogrammetric suites like Intergraph's ImageStation, the Photogrammeter had to manually register (click with a mouse or pointer) all the remarkable points in an image, such that the 8 red circles imprinted on classical 23cm by 23cm aerial photographs (defining 4 axes, which intersect all at the geometric center of the photograph, see Figure 1.1). The centers of such circles are called the fiducial centers of the image. Moreover, the position and the orientation of the plane were known from the Global Navigation Satellite System (GPS, Glonass, Beidou, Galileo) and the Inertial Measurement Unit. In nowadays photographic camera images, such fiducial centers are not usually present. Moreover, modern cameras are not tight to a plane or a GNSS device and an Inertial Measurement Unit.



Figure 1.1: A classical example of aerial photogrammetric camera photograph. *Source:* [1]

In this thesis we consider the fully deterministic distortion correction of a modern camera with control of the uncertainty and without knowledge of any geometric information on the position and the orientation of the camera, corresponding to the modern non-photogrammetric digital camera based mapping. For this purpose, we need to obtain photographs, whose scale is constant (unlike normal photographs and like orthophotographs), because they correspond to the orthogonal projection that maps each point $(x, y, z) \in \mathbb{R}^3$ into the point $(x, y) \in \mathbb{R}^2$, in order for us to perform geometric measurements directly on the orthophotograph (see Figure 1.2) for the difference between the perspective projection of normal photographs and the orthogonal projection of orthophotographs). However, unlike orthophotographs, these photographs were not corrected of all geometric flaws that affect a photograph.

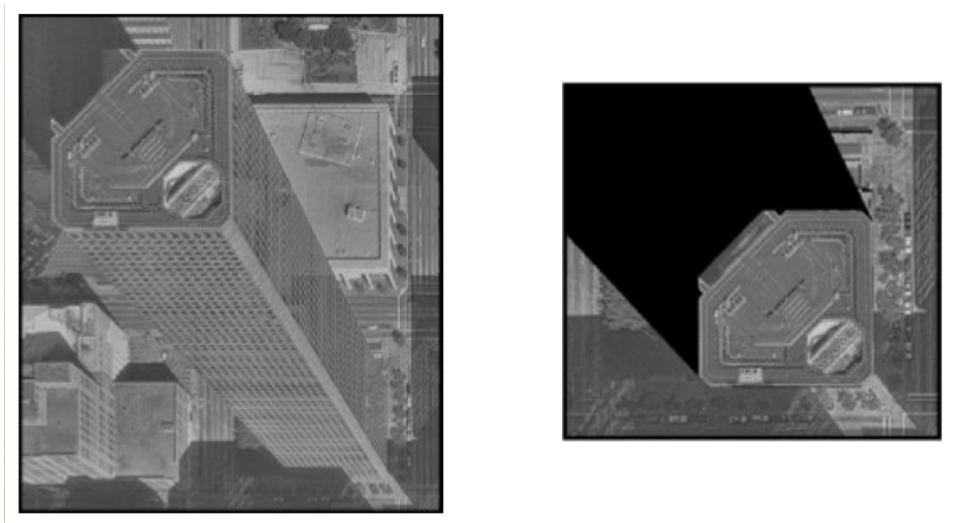


Figure 1.2: The difference between the perspective projection of normal photographs and the orthogonal projection of orthophotographs

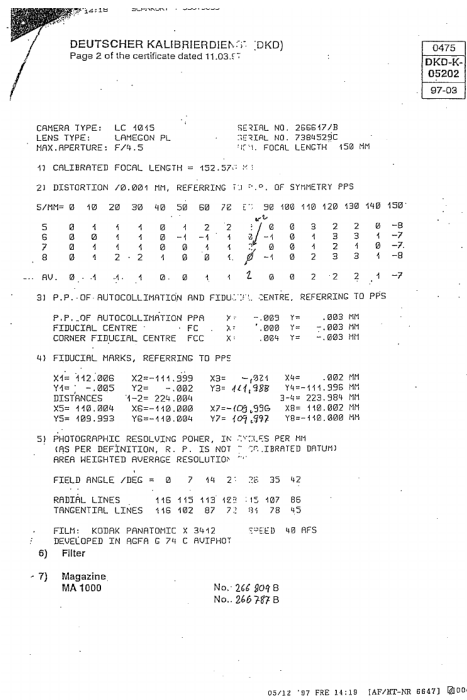
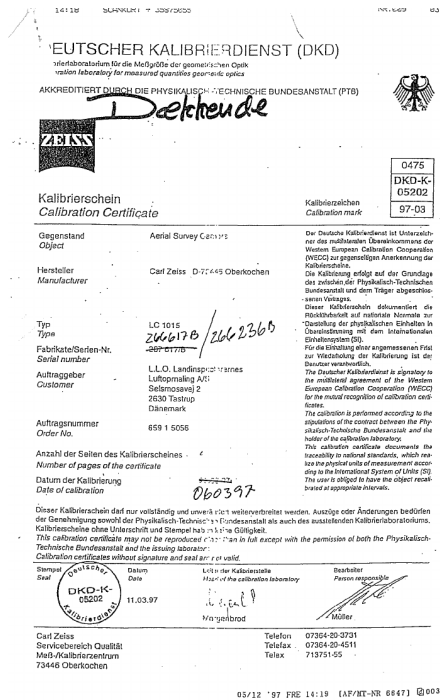


Figure 1.3: First pages of a Zeiss calibration report from Denmark's Kort og Matrikel Styrelsen

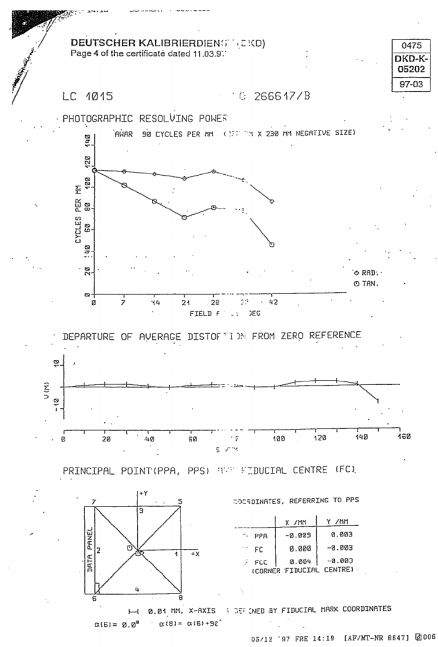
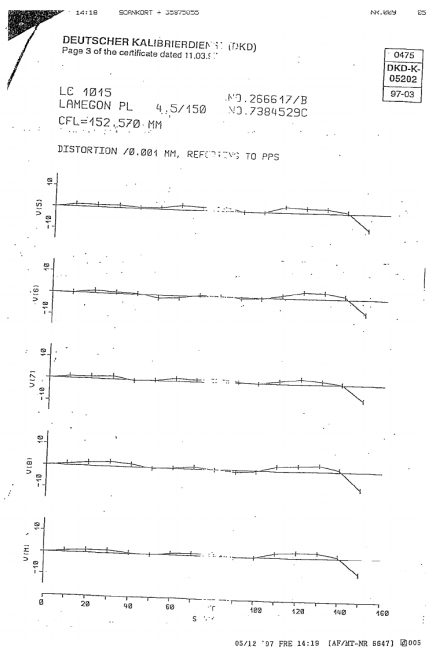


Figure 1.4: Last pages of the same Zeiss calibration report from Denmark's Kort og Matrikel Styrelsen

1.2 Justification and Contribution

The problem of non-determinism of automated calibration algorithms is very important for Photogrameters, who, as a profession, have always relied and must rely only on deterministic algorithms. This situation is similar to the insurance companies, who refuse to cover autonomous cars, as long as they rely on non-deterministic algorithms. The non-determinism infringes the reliable nature of Photogrammetric measurements in the American Society for Photogrammetry and Remote Sensing (ASPRS) definition of Photogrammetry.

Photogrammetric measurements are used in many decision taking activities based on measurements, in civil engineering [10], construction [11], forensics [12], surgery [13], astronomy [14], real estate [15], in addition to the classical related disciplines of geodesy [16], applied topography [17], and metrology [18].

The main geometric flaw that affects all high quality imaging is the distortion [19]. Among the different kinds of distortion, the radial distortion is the one whose amplitude is the greatest (see [20]).

In this thesis, a comparison between different polynomial interpolation techniques and models to the fully deterministic radial distortion correction is made. It is based on the precise pixel level manual feature measurements. These methods and models can be broadly classified into linear ones, piecewise cubic ones and higher degree ones, and they all assume only the continuity of the function that maps radial distances to radial distortion and its correction.

1.3 Objectives

1.3.1 General Objective

To provide a comparative analysis of the radial distortion calibration of digital cameras using different algebraic methods without the use of non-deterministic algorithms.

1.3.2 Specific Objectives

- To determine the feature points of a photographic image without the use of non-deterministic algorithms.
- To compare different algebraic methods and determine which one gives the best correction of the radial distortion.
- To propose an algebraic method of calibration of radial distortion based on the results obtained.

1.4 Document organization

An introductory theoretical background with a quick review of some photogrammetry concepts and the data fitting algebraic methods used in this work is presented in Chapter 2.

The methodology used in this study is detailed in Chapter 3. It includes a description of the lattice, photos and feature detection method used as well as the full description of the experiments.

The results are shown, compared and discussed through comparative tables and plots in Chapter 4.

The conclusions obtained from this work and some recommendation for future works that can improve it are presented in Chapter 5.

Some supplementary material is presented in Appendix A.

Chapter 2

Theoretical Framework

This chapter presents an introductory theoretical background with a broad review of the concepts applied in this work. It presents a quick review of some photogrammetry concepts and the data fitting methods used in this work.

2.1 Pinhole Camera Model

Based in the book *Image Analysis, Vision and Computer Graphics* by Jens M. Cartensen [2], the bundle of light rays from the object passes through the projection center (the lens center) to then, be pictured on the image plane (Figure 3.1).

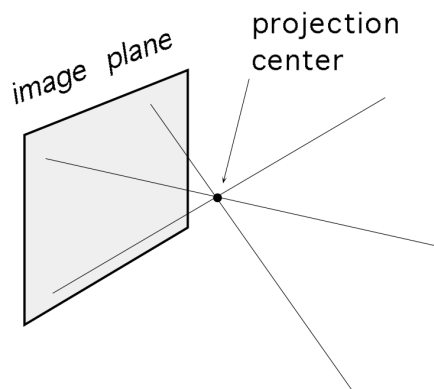


Figure 2.1: Projection center and image plane. *Source:* [2]

The ideal model for image acquisition in cameras is known as the pinhole camera

model. This model consists of an airtight box with a very fine hole (projection center) through which the light rays enter and then, get projected on the image plane. Ideally, the hole should be so narrow to allow only the bundle of light rays to pass through as straight unbroken light rays.

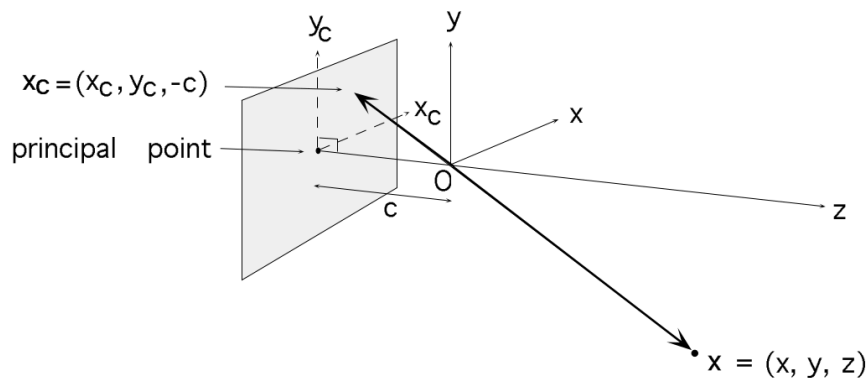


Figure 2.2: Pinhole Camera Geometry. *Source:* [2]

The geometry of the pinhole camera is shown in Figure 3.2. The *principal point* is the orthogonal projection of the *perspective or projection center* (O) onto the *image plane*. If the manufacturing process of the lenses and of the camera were perfect, the principal point would be the intersection of the *optical axis (of symmetry)* and the image plane. The *camera constant* (c) is the distance between the principal point and the *perspective or projection center* (O). A *camera coordinate system* can be seen with its origin in the projection center, the x and y axes are parallel to the image plane, and the z axis is the axis joining the principal point and the projection center. Finally, x is the real world point with coordinates (x, y, z) , x_c is the image point with coordinates (x_c, y_c) , [2].

2.2 The Lens System

As just described, the pinhole camera model is an ideal model and it has a very fine hole. This hole does not allow enough light to generate clear-cut images. Therefore, a lens system is needed to produce the central projection.

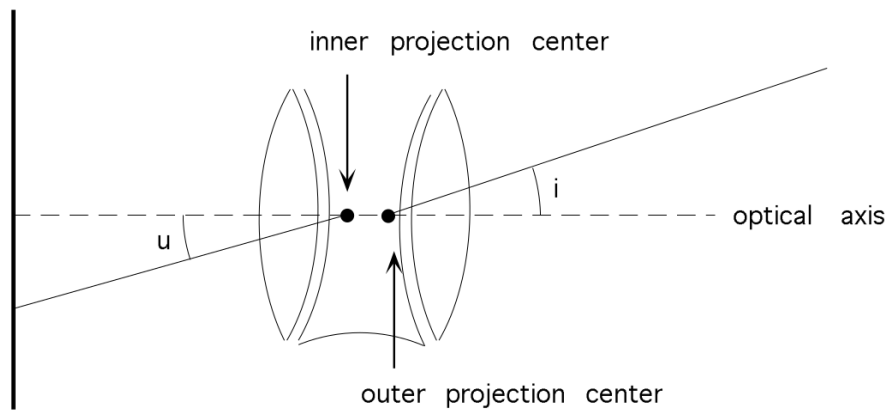


Figure 2.3: Lens System. *Source:* [2]

Figure 3.3 describes a lens system. In order to describe the path of the rays through the lens system, two virtual projection centers known as inner and outer projection centers or front and rear nodal points are introduced.

The front and rear nodal points “*have the property that a ray aimed at one of them will be refracted by the lens such that it appears to have come from the other, and with the same angle with respect to the optical axis*” [21].

Lens distortion

In a distortion free camera, like the pinhole camera, the incidence ray and outgoing ray lie in a plane through the optical axis and the angle between them and the optical axis is the same, in other words, angle i is equal to angle u . But, in real world cameras, this is not the case due to the geometric shape of the lenses. Then, lens distortion must be taken into account.

Lens distortion is made up mainly of two types: radial and tangential distortion (Figure 3.4). Radial distortion refers to the displacement of the point P (without distortion or ideal position) to a new position P' in the image that moves on the line that connects the point with the geometric center of the image (O) also known as the center of distortion. Optically, radial distortion takes place when the angle of the outgoing ray is different from the angle of incident ray. Tangential distortion is the displacement of the point P in

a perpendicular direction to the line that joins the center of distortion with that point. Optically, tangential distortion occurs when the incidence and outgoing ray do not lie in the same plane containing the optical axis, [2]. Note that the center of distortion is invariant to both transformations in the images. Because of the lens production methods, the radial distortion is by far the largest while tangential distortion is usually less than a few microns and it will not be specifically treated in this work.

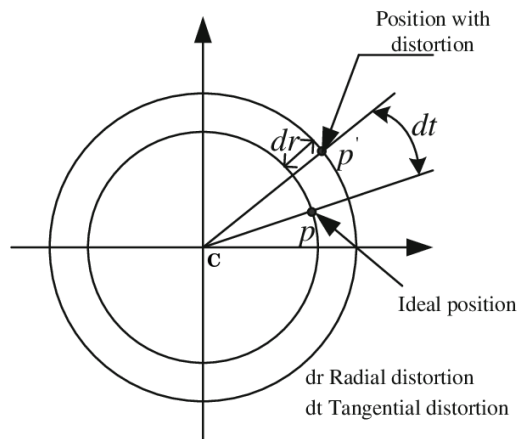


Figure 2.4: Radial and Tangential Distortion. *Source:* [3]

According to [2], the radial distortion dr can be expressed as an odd exponents polynomial in r to the powers of one to seven:

$$dr = a_1 r + a_2 r^3 + a_3 r^5 + a_4 r^7, \quad (2.1)$$

where: a_i are the distortion coefficients and r is the radial distance of the distorted image point.

The radial distance is the Euclidean distance from the geometric center of the image C to a point P :

$$r = \sqrt{(x_p - x_c)^2 + (y_p - y_c)^2} \quad (2.2)$$

where: x_p and y_p are the coordinates of the point P . x_c and y_c are the coordinates of the

geometric center of the image.

Figure 3.4 also shows another way to define the radial distortion dr :

$$dr = r_d - r_u, \quad (2.3)$$

where: r_d is the radial distance of the distorted image point, and r_u is the radial distance of the undistorted image point.

2.3 Mathematical Model

A mathematical model is a description or representation of a system using mathematical concepts and language [22].

A mathematical model is deterministic when there is no probabilistic component. Our methods are deterministic because its machinery is fully algebraic. That is, the input received by the method will always produce the same result. In addition, the code was made in Maxima [23], a fairly complete computer algebra system written in the functional programming language Lisp with an emphasis on symbolic computation.

2.4 Data Fitting Algebraic Methods

In this section, we will describe 4 data fitting algebraic methods:

2.4.1 Minimize the sum of squares of the vertical distance

Residual (ϵ)

This algebraic method tries to minimize the sum of the squares of the vertical distance between the actual value of y and the model predicted value of y . We are going to define

this as the residual:

$$\epsilon = y - \hat{y} = y - Xb = \Delta y, \quad (2.4)$$

where y is the observed value of the radial distortion, \hat{y} is the modeled value of the radial distortion, X is the matrix formed by the odd powers of the radial distances and b is the unknown vector of coefficients.

Consider the following model of the form

$$y = \beta_0 + \beta_1 X_1 \beta_2 X_2 + \dots + \beta_k X_k + \epsilon \quad (2.5)$$

where: ϵ is the residual.

Assume that (2.5) is the model of an experiment with n observations. Then, the n -tuples of observations are also assumed to follow the same model:

$$\begin{aligned} y_1 &= \beta_0 + \beta_1 X_{11} \beta_2 X_{12} + \dots + \beta_k X_{1k} + \epsilon_1 \\ y_2 &= \beta_0 + \beta_1 X_{21} \beta_2 X_{22} + \dots + \beta_k X_{2k} + \epsilon_2 \\ &\vdots \\ y_n &= \beta_0 + \beta_1 X_{n1} \beta_2 X_{n2} + \dots + \beta_k X_{nk} + \epsilon_n \end{aligned}$$

These equations can also be written in matrix form:

$$\begin{bmatrix} y_1 \\ y_2 \\ \vdots \\ y_n \end{bmatrix} = \begin{bmatrix} 1 & x_{11} & x_{12} & \dots & x_{1k} \\ 1 & x_{21} & x_{22} & \dots & x_{2k} \\ \vdots & \vdots & \vdots & & \vdots \\ 1 & x_{n1} & x_{n2} & \dots & x_{nk} \end{bmatrix} \begin{bmatrix} \beta_0 \\ \beta_1 \\ \vdots \\ \beta_k \end{bmatrix} + \begin{bmatrix} \epsilon_1 \\ \epsilon_2 \\ \vdots \\ \epsilon_n \end{bmatrix}$$

or:

$$y = X\beta + \epsilon \quad (2.6)$$

This method tries to find estimated values for β in order to provide the “best” fit for the data points. These estimators are obtained by minimizing the sum of squared residuals

ϵ_i . This means:

$$\text{Find } \min_{\beta} S(\beta) \text{ for } S(\beta) = \sum_i^N \epsilon_i^2 = \sum_i^n (y_i - (\beta x_i))^2.$$

Parameters Estimation

The Parameter Estimation is an algebraic deterministic process.

Let B be the set of all possible values of β . As described above, the purpose is to find a vector $b = [b_1, b_2, \dots, b_k]$ from B that minimizes the sum of squared deviations of ϵ :

$$S(\beta) = \sum_{i=1}^n \hat{\epsilon}_i^2 = \epsilon^\top \epsilon = (y - X\beta)^\top (y - X\beta). \quad (2.7)$$

Then,

$S(\beta)$ can be written as:

$$S(\beta) = y^\top y + \beta^\top X^\top X \beta - 2\beta^\top X^\top y \quad (2.8)$$

. As $S(\beta)$ is a quadratic form, it does not have a maximum, nor an inflexion point, and it has only global minimum value. Thus, its attained global minimum value corresponds to the root of its derivative. Differentiate $S(\beta)$ with respect to β :

$$\frac{\partial S(\beta)}{\partial \beta} = 2X^\top X \beta - 2X^\top y = 2(X^\top X \beta - X^\top y) \quad (2.9)$$

$$\frac{\partial^2 S(\beta)}{\partial \beta^2} = 2X^\top X. \quad (2.10)$$

Equation (2.9) is equal to zero if and only if:

$$X^\top X b = X^\top y. \quad (2.11)$$

In the case in which the $\text{rank}(X)=k$ (full rank), we know that $X^\top X$ is positive definite

and non-singular. Subsequently, the unique solution for b is:

$$b = (X^T X)^{-1} X^T y. \quad (2.12)$$

Being that $\frac{\partial^2 S(\beta)}{\partial \beta^2}$ is at least non-negative definite, which means that $\frac{\partial^2 S(\beta)}{\partial \beta^2} > 0$, then b minimizes $S(\beta)$.

2.4.2 Minimize the sum of squares of the orthogonal distance

Residual (ϵ)

This algebraic method tries to minimize the sum of the squares of the orthogonal distance between the actual value of y and the model. Then, the residual is defined as follows:

$$\epsilon = V \cdot \vec{N}. \quad (2.13)$$

where: V is the matrix of the difference of y ($\Delta y = y - \hat{y}$) and \vec{N} is the Unitary Normal Vector.

The matrix V and the \vec{N} vector are defined as follows:

$$V = \begin{bmatrix} 0 & 0 & 0 & 0 & 0 & \Delta y_1 \\ 0 & 0 & 0 & 0 & 0 & \Delta y_2 \\ \vdots & \vdots & \vdots & \vdots & \vdots & \vdots \\ 0 & 0 & 0 & 0 & 0 & \Delta y_n \end{bmatrix}, \quad (2.14)$$

$$\vec{N} = \frac{1}{\sqrt{\beta_1^2 + \beta_2^2 + \dots + \beta_k^2 + 1}} \begin{bmatrix} \beta_1 \\ \beta_2 \\ \vdots \\ \beta_k \\ -1 \end{bmatrix}. \quad (2.15)$$

As in the previous method, the system of equations of the model for n observations can be written in a matrix way as follows:

$$y = X\beta + \epsilon. \quad (2.16)$$

This method tries to find estimated values for β in order to provide the “best” fit for the data points. These estimators are obtained by minimizing the sum of squared residuals $\hat{\epsilon}_i$. This means another minimization problem:

$$\text{Find } \min_{\beta} S(\beta) \text{ for } S(\beta) = \sum_i^N \epsilon_i^2 = \epsilon^\top \epsilon = (V \cdot \vec{N})^\top (V \cdot \vec{N}).$$

Parameter Estimation

In order to talk about the Parameter Estimation of this model, it is necessary to understand its geometry.

Figure 2.5 shows the geometry of one observed point and the hyperplane of the model. It demonstrates that the angle α_1 between the unitary normal vector and the vector of the vertical distance in y will be constant for each observed point. Also, the angle α_2 between the normal and the hyperplane is always 90° . Then, by definition, all the three angles of each triangle formed between the observed point and its vertical and orthogonal projections onto the hyperplane of the model, α_1 , α_2 , α_3 , are the same for each observed point. Therefore, we can conclude that the parameter estimation for this method is the same as the one detailed for the minimization problem of the vertical distance, but the residual is different for each model.

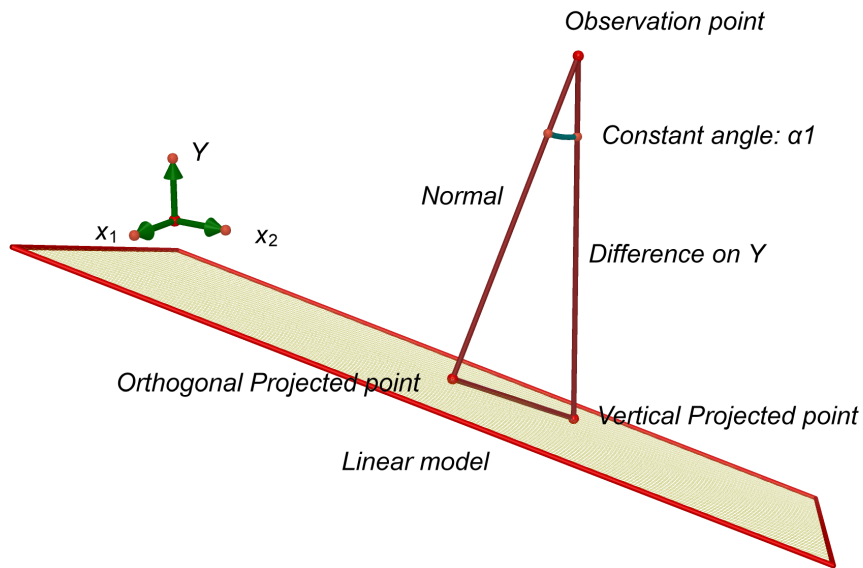


Figure 2.5: Orthogonal distance vs Vertical Distance

2.4.3 Cubic Spline Interpolation

The following subsection is based on [24]. Cubic Spline Interpolation is a method of Spline Interpolation which gives a smoother interpolating polynomial than the preceding methods.

Given a set of n data points (x_i, y_i) , $i = 1, \dots, n$ in an interval $[a, b]$, the idea is to find a piecewise cubic polynomial of the form:

$$S(x) = \begin{cases} s_1(x) & \text{if } x_1 \leq x < x_2 \\ s_2(x) & \text{if } x_2 \leq x < x_3 \\ \vdots & \\ s_{n-1} & \text{if } x_{n-1} \leq x \leq x_n \end{cases}, \quad (2.17)$$

where each cubic polynomial s_i is a third degree polynomial defined by:

$$S_i(x) = a_i(x - x_i)^3 + b_i(x - x_i)^2 + c_i(x - x_i) + d_i \quad \text{for } i = 1, 2, \dots, n - 1. \quad (2.18)$$

To determine this cubic spline $S(x)$, these equations are determined by the following conditions:

1. $S(x)$ must interpolate all data points and so in each sub interval. Then, we must have $S_i(x_i) = y_i$ and $S_i(x_{i+1}) = y_{i+1}$.
2. $S'(x)$ must be continuous at each of the internal knots. Therefore, we must have $S'_{i-1}(x_i) = S'_i(x_i)$.
3. $S''(x)$ must be continuous at each of the internal knots. Therefore, we must have $S''_{i+1}(x_i) = S''_i(x_i)$.
4. One of the following conditions at the end points a and b :
 - Natural Spline: $S''_0(a) = 0 = S''_n(b)$.
 - Clamped cubic Spline: $S''_0(a) = f''(a)$ and $S''_n(b) = f''(b)$.

Parameter Estimation

The first and second derivative of (2.20) are fundamental to solve this problem, and they are:

$$S'_i(x) = 3a_i(x - x_i)^2 + 2b_i(x - x_i) + c_i, \quad (2.19)$$

$$S''_i(x) = 6a_i(x - x_i) + 2b_i, \quad (2.20)$$

for $i = 1, 2, \dots, n - 1$.

Due to condition 1, we have that:

$$S(x_i) = y_i \quad \text{for } i = 1, 2, \dots, n-1. \quad (2.21)$$

Since $x_i \in [x_i, x_{i+1}]$, $S(x_i) = s_i(x_i)$ we have:

$$\begin{aligned} y_i &= s_i(x_i) \\ &= a_i(x_i - x_i)^3 + b_i(x_i - x_i)^2 + c_i(x_i - x_i) + d_i \\ &= d_i. \end{aligned} \quad (2.22)$$

Since the curve $S(x)$ must be continuous across its entire interval, it can be concluded that each spline must join at the data points, so:

$$S_i(x_i) = S_{i-1}(x_i) \quad \text{for } i = 2, \dots, n. \quad (2.23)$$

From (2.18) we have:

$$d_i = a_{i-1}(x_i - x_{i-1})^3 + b_{i-1}(x_i - x_{i-1})^2 + c_{i-1}(x_i - x_{i-1}) + d_{i-1} \quad \text{for } i = 2, \dots, n-1. \quad (2.24)$$

Letting $h = x_i - x_{i-1}$ and replacing it in (2.24):

$$d_i = a_{i-1}h^3 + b_{i-1}h^2 + c_{i-1}h + d_{i-1} \quad \text{for } i = 2, \dots, n-1. \quad (2.25)$$

Due to condition 2, we have:

$$S'_{i-1}(x_i) = S'_i(x_i). \quad (2.26)$$

And by (2.19), we know that:

$$\begin{aligned} s'_i(x_i) &= c_i, & \text{and} \\ s'_{i-1}(x_i) &= 3a_{i-1}(x_i - x_{i-1})^2 + 2b_{i-1}(x_i - x_{i-1}) + c_{i-1}. \end{aligned} \quad (2.27)$$

So,

$$c_i = 3a_{i-1}(x_i - x_{i-1})^2 + 2b_{i-1}(x_i - x_{i-1}) + c_{i-1}. \quad (2.28)$$

Again, letting $h = x_i - x_{i-1}$ and replacing it in (2.28):

$$c_i = 3a_{i-1}h^2 + 2b_{i-1}h + c_{i-1} \quad \text{for } i = 2, \dots, n-1. \quad (2.29)$$

From (2.20), we have:

$$\begin{aligned} S_i''(x) &= 6a_i(x - x_i) + 2b_i, \\ S_i''(x_i) &= 6a_i(x_i - x_i) + 2b_i, \\ S_i''(x_i) &= 2b_i \quad \text{for } i = 2, \dots, n-2. \end{aligned} \quad (2.30)$$

Lastly, due to condition 3, we know that $S_{i+1}''(x_i) = S_i''(x_i)$, for $i = 1, 2, \dots, n-1$. Then,

$$S_i''(x_{i+1}) = 6a_i(x_{i+1} - x_i) + 2b_i, \quad (2.31)$$

$$S_{i+1}''(x_{i+1}) = 6a_i(x_{i+1} - x_i) + 2b_i. \quad (2.32)$$

Letting $h = x_{i+1} - x_i$ and using (2.30) and (3.32) we have:

$$\begin{aligned} S_{i+1}''(x_{i+1}) &= 6a_i(x_{i+1} - x_i) + 2b_i, \\ 2b_{i+1} &= 6a_i h + 2b_i. \end{aligned} \quad (2.33)$$

In order to simplify these equations and make the determination of a_i , b_i , c_i and d_i easier, we are going to substitute $S_i''(x_i)$ for M_i and express the above equations in terms of M_i and y_i .

Each b_i can be represented by:

$$\begin{aligned} s_i''(x_i) &= 2b_i, \\ M_i &= 2b_i, \\ b_i &= \frac{M_i}{2}, \end{aligned} \tag{2.34}$$

and d_i has already been determined to be

$$d_i = y_i. \tag{2.35}$$

Similarly, using (2.33), a_i can be redefined as

$$\begin{aligned} 2b_{i+1} &= 6a_i h + 2b_i, \\ 6a_i h &= 2b_{i+1} - 2b_i, \\ a_i &= \frac{2b_{i+1} - 2b_i}{6h}, \\ a_i &= \frac{2\left(\frac{M_{i+1}}{2}\right) - 2\left(\frac{M_i}{2}\right)}{6h}, \\ a_i &= \frac{M_{i+1} - M_i}{6h}, \end{aligned} \tag{2.36}$$

and c_i can be redefined as:

$$\begin{aligned}
d_{i+1} &= a_i h^3 + b_i h^2 + c_i h + d_i, \\
c_i h &= -a_i h^3 - b_i h^2 - d_i + d_{i+1}, \\
c_i &= \frac{-a_i h^3 - b_i h^2 - d_i + d_{i+1}}{h}, \\
c_i &= \frac{-a_i h^3 - b_i h^2}{h} + \frac{-d_i + d_{i+1}}{h}, \\
c_i &= (-a_i h^2 - b_i h) - \frac{d_i - d_{i+1}}{h}, \\
c_i &= -\left(\frac{M_{i+1} - M_i}{6h} h^2 + \frac{M_i}{2} h\right) - \frac{y_i - y_{i+1}}{h}, \\
c_i &= \frac{y_{i+1} - y_i}{h} - \left(\frac{M_{i+1} - M_i}{6} h + \frac{3M_i}{6} h\right), \\
c_i &= \frac{y_{i+1} - y_i}{h} - \left(\frac{M_{i+1} - M_i + 3M_i}{6}\right)h, \\
c_i &= \frac{y_{i+1} - y_i}{h} - \left(\frac{M_{i+1} + 2M_i}{6}\right)h.
\end{aligned} \tag{2.37}$$

Then, the equation for determining our parameters for the $n - 1$ equations are:

$$\begin{aligned}
a_i &= \frac{M_{i+1} - M_i}{6h}, \\
b_i &= \frac{M_i}{2}, \\
c_i &= \frac{y_{i+1} - y_i}{h} - \left(\frac{M_{i+1} + 2M_i}{6}\right)h, \\
d_i &= y_i.
\end{aligned} \tag{2.38}$$

In order to make it easier to handle, by (2.29) and (2.38):

$$\begin{aligned}
c_{i+1} &= 3a_i h^2 + 2b_i h + c_i, \\
\frac{y_{i+2} - y_{i+1}}{h} - \left(\frac{M_{i+2} + 2M_{i+1}}{6}\right)h &= 3\frac{M_{i+1} - M_i}{6h}h^2 + 2\frac{M_i}{2}h + \frac{y_{i+1} - y_i}{h} - \left(\frac{M_{i+1} + 2M_i}{6}\right)h, \\
\frac{y_{i+2} - y_{i+1}}{h} - \frac{y_{i+1} - y_i}{h} &= 3\frac{M_{i+1} - M_i}{6h}h^2 + 2\frac{M_i}{2}h + \left(\frac{M_{i+2} + 2M_{i+1}}{6}\right)h - \left(\frac{M_{i+1} + 2M_i}{6}\right)h, \\
\frac{y_{i+2} - 2y_{i+1} + y_i}{h} &= h\left(\frac{3M_{i+1} - 3M_i}{6} + \frac{6M_i}{6} - \left(\frac{M_{i+1} + 2M_i}{6}\right) + \left(\frac{M_{i+2} + 2M_{i+1}}{6}\right)\right), \\
\frac{y_{i+2} - 2y_{i+1} + y_i}{h} &= \frac{h}{6}(M_i + 4M_{i+1} + M_{i+2}), \\
6\left(\frac{y_{i+2} - 2y_{i+1} + y_i}{h^2}\right) &= M_i + 4M_{i+1} + M_{i+2}, \\
\text{for } i &= 1, \dots, n-1.
\end{aligned} \tag{2.39}$$

And these systems can be put in the following matrix equation:

$$\begin{bmatrix}
1 & 4 & 1 & 0 & \cdots & 0 & 0 & 0 & 0 \\
0 & 1 & 4 & 1 & \cdots & 0 & 0 & 0 & 0 \\
0 & 0 & 1 & 4 & \cdots & 0 & 0 & 0 & 0 \\
\vdots & \vdots & \vdots & \vdots & \ddots & \vdots & \vdots & \vdots & \vdots \\
0 & 0 & 0 & 0 & \cdots & 4 & 1 & 0 & 0 \\
0 & 0 & 0 & 0 & \cdots & 1 & 4 & 1 & 0 \\
0 & 0 & 0 & 0 & \cdots & 0 & 1 & 4 & 1 \\
& & & & & & & & M_n
\end{bmatrix}
\begin{bmatrix}
M_1 \\
M_2 \\
M_3 \\
M_4 \\
\vdots \\
M_{n-3} \\
M_{n-2} \\
M_{n-1} \\
M_n
\end{bmatrix}
= \frac{6}{h^2}
\begin{bmatrix}
y_3 - 2y_2 + y_1 \\
y_4 - 2y_3 + y_2 \\
y_5 - 2y_4 + y_3 \\
\vdots \\
y_{n-2} - 2y_{n-3} + y_{n-4} \\
y_{n-1} - 2y_{n-2} + y_{n-3} \\
y_n - 2y_{n-1} + y_{n-2}
\end{bmatrix}. \tag{2.40}$$

Note that the system has $n - 2$ rows and n columns and therefore, it is an under-determined system. In order to generate a unique cubic spline, the condition 4, which gives the condition at the end points a and b , must be taken into account. In this thesis, we will be working with natural splines only:

Natural Splines:

This spline has the constraint that the second derivative should be equal to zero at the end points:

$$M_1 = M_n = 0. \quad (2.41)$$

This results in the spline extending as a straight line outside the endpoints. The matrix for determining the $M_1 - M_n$ values can be adapted as follows:

$$\begin{bmatrix} 1 & 0 & 0 & 0 & \cdots & 0 & 0 & 0 & 0 \\ 0 & 1 & 4 & 1 & \cdots & 0 & 0 & 0 & 0 \\ 0 & 0 & 1 & 4 & \cdots & 0 & 0 & 0 & 0 \\ \vdots & \vdots & \vdots & \vdots & \ddots & \vdots & \vdots & \vdots & \vdots \\ 0 & 0 & 0 & 0 & \cdots & 4 & 1 & 0 & 0 \\ 0 & 0 & 0 & 0 & \cdots & 1 & 4 & 1 & 0 \\ 0 & 0 & 0 & 0 & \cdots & 0 & 0 & 0 & 1 \end{bmatrix} \begin{bmatrix} 0 \\ M_2 \\ M_3 \\ M_4 \\ \vdots \\ M_{n-3} \\ M_{n-2} \\ M_{n-1} \\ 0 \end{bmatrix} = \frac{6}{h^2} \begin{bmatrix} y_1 - 2y_2 + y_3 \\ y_2 - 2y_3 + y_4 \\ y_3 - 2y_4 + y_5 \\ \vdots \\ y_{n-4} - 2y_{n-3} + y_{n-2} \\ y_{n-3} - 2y_{n-2} + y_{n-1} \\ y_{n-2} - 2y_{n-1} + y_n \end{bmatrix}. \quad (2.42)$$

Eliminating the first and last column and row of this matrix, we have:

$$\begin{bmatrix} 4 & 1 & 0 & \cdots & 0 & 0 & 0 \\ 1 & 4 & 1 & \cdots & 0 & 0 & 0 \\ 0 & 1 & 4 & \cdots & 0 & 0 & 0 \\ \vdots & \vdots & \vdots & \ddots & \vdots & \vdots & \vdots \\ 0 & 0 & 0 & \cdots & 4 & 1 & 0 \\ 0 & 0 & 0 & \cdots & 1 & 4 & 1 \\ 0 & 0 & 0 & \cdots & 0 & 1 & 4 \end{bmatrix} \begin{bmatrix} M_2 \\ M_3 \\ M_4 \\ \vdots \\ M_{n-3} \\ M_{n-2} \\ M_{n-1} \end{bmatrix} = \frac{6}{h^2} \begin{bmatrix} y_1 - 2y_2 + y_3 \\ y_2 - 2y_3 + y_4 \\ y_3 - 2y_4 + y_5 \\ \vdots \\ y_{n-4} - 2y_{n-3} + y_{n-2} \\ y_{n-3} - 2y_{n-2} + y_{n-1} \\ y_{n-2} - 2y_{n-1} + y_n \end{bmatrix}. \quad (2.43)$$

This result gives an $n - 2$ by $n - 2$ matrix, which will determine the solutions for M_2 through M_{n-1} . The spline is now unique.

Residual

The residual of this model is calculated with the the orthogonal distance, which is the distance of the observed points to the nearest point of each spline. It is defined as follows:

$$\begin{aligned}
 S(x) &= P_{cs}(x, y) \\
 normal &= \frac{\partial P_{cs}(x, y)}{\partial x}(x_0 - x) + \frac{\partial P_{cs}(x, y)}{\partial y}(y_0 - y) \\
 \epsilon &= \min_{(x,y) \in V(\{S(x), normal\})} d_E((x_0, y_0), (x, y))
 \end{aligned} \tag{2.44}$$

where: $P_{cs}(x, y)$ is the polynomial obtained with Cubic Spline interpolation, d_E is the Euclidean distance and $V(PS)$ stands for the set of common roots (or variety) of the polynomial set PS .

2.4.4 Wu's polynomial elimination

Wu's method is an algorithm for eliminating variables from systems of multivariate polynomial equations by means of converting such systems into equivalent triangular sets, which uses polynomial division and only requires pseudo-remainder computations [25]. In other words, Wu's Method transforms a system of polynomial equations into an equivalent triangular system of polynomial equations using the Euclidean Division Algorithm:

Let $K[x_c]$ be the ring of polynomials in the variable x_c , i.e., the set of polynomials in the variable x_c , equipped with the addition of polynomials and the multiplication of polynomials, such that the set of polynomials in the variable x_c together with the addition of polynomials is a group, the set of polynomials in the variable x_c has a neutral element for the multiplication of polynomials and the multiplication of polynomials is well formed and associative, and the multiplication of polynomials is distributive with respect to the addition of polynomials.

Let p and q be two polynomials considered as univariate in the variable to be eliminated x_c :

$$\exists Q, R \in K[x_c] \quad p = q \cdot Q + R \quad \text{where} \quad \deg(R, x_c) < \deg(q, x_c). \quad (2.45)$$

A more detailed definition could be find in Appendix A.

Residual

The residual of this model is calculated with the orthogonal distance as in the previous method, which is the distance of the observed points to the nearest point of the model. It is defined as follows:

$$\begin{aligned} S(x) &= P_{Wu}(x, y) \\ normal &= \frac{\partial P_{Wu}(x, y)}{\partial x}(x_0 - x) + \frac{\partial P_{Wu}(x, y)}{\partial y}(y_0 - y) \\ \epsilon &= \min_{(x, y) \in V(\{S(x), normal\})} d_E((x_0, y_0), (x, y)) \end{aligned} \quad (2.46)$$

where: P_{Wu} is the polynomial obtained using Wu's Method and d_E is the Euclidean distance.

2.4.5 Legendre Polynomials Approximation

According to Weierstrass Approximation Theorem [26] any continuous function in a closed interval $[a, b]$ can be approximated by lineal combinations of polynomials within the interval. The Legendre polynomials form an orthogonal set of polynomials and they can be obtained as follows [27]:

$$P_n(x) = \frac{1}{n!2^n} \frac{d^n}{dx^n} (x^2 - 1)^n, \quad \text{for } n = 0, 1, 2, \dots \quad (2.47)$$

2.5 Error Measure

The error present in each model is evaluated by two different and complementary measures: the root mean square error and the maximum error.

2.5.1 Root Mean Square Error

The RMS value of vector can be a popular measure for the performance and the accuracy of a model [28]. It is defined as follows:

$$RMS = \sqrt{\frac{1}{n} \sum_{i=1}^n \epsilon_i^2}. \quad (2.48)$$

where: ϵ is the residual vector of each method and n is the number of data points.

2.5.2 L-infinity Norm

A common used vector norm is the magnitude of the largest component of the vector, called L-infinity Norm. It is defined as follows [29]:

$$\|\epsilon\|_{\infty} = \max_i |\epsilon_i| y_{ui} = \text{hackery}_c + \Delta_y * K_y \quad \text{for } i = 1, \dots, 81. \quad (2.49)$$

Chapter 3

Methodology

In the present chapter, the experimental set up and the concepts of Chapter 2 will be applied to address the problem. First, a description of the lattice used will be given. Then, an explanation of the orthophotographs and the method for feature Points Detection will be detailed. Finally, a detailed description of the experiments made in this work will be provided.

3.1 Lattice

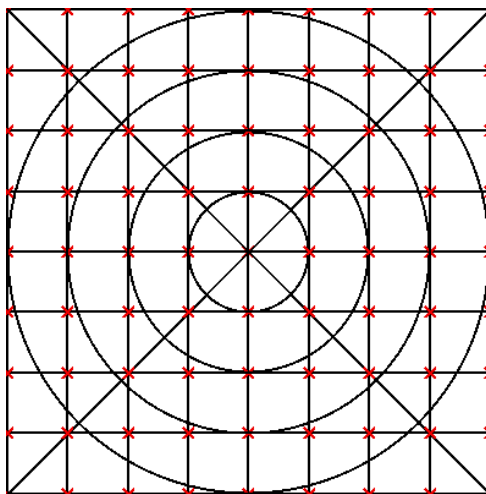


Figure 3.1: Lattice pattern image produced by GeoGebra.

The lattice pattern image (Figure 3.1) that contains many feature points with different distances from the image center was created using GeoGebra. The size in pixels of the image was 397x398. It was glued to a wooden cube of 14x14 cm, to then, be photographed with the camera.

In equations detailed in this chapter, it will be useful to know the constant distance/-variation of the coordinates in x and y between each feature point of this lattice. Since the lattice is formed by 8x8 identical squares of the same size, then this measure is defined as follows:

$$\begin{aligned}\Delta_x &= \frac{397}{8} = 49,625 \\ \Delta_y &= \frac{398}{8} = 49,75\end{aligned}\tag{3.1}$$

3.2 Orthophoto

An orthophoto or orthophotograph is a photograph geometrically corrected such that the scale is uniform (this means that the photo follows a given map projection) and the distortion and other geometric artifacts have been corrected.

In this thesis, in order to compute the radial distortion, we needed to use photographs with a constant scale, that can be used to measure the true distance of features within the photography. In the remainder of this thesis experiments, we will refer them as orthophotos or orthophotographs.

Figures 3.2 and 3.3 show the two orthophotographs used in this work. The pixel size of both photos is 5184x3888. Then, the coordinates of the geometric center are:

$$(x_c, y_c) = (2592, 1994)\tag{3.2}$$

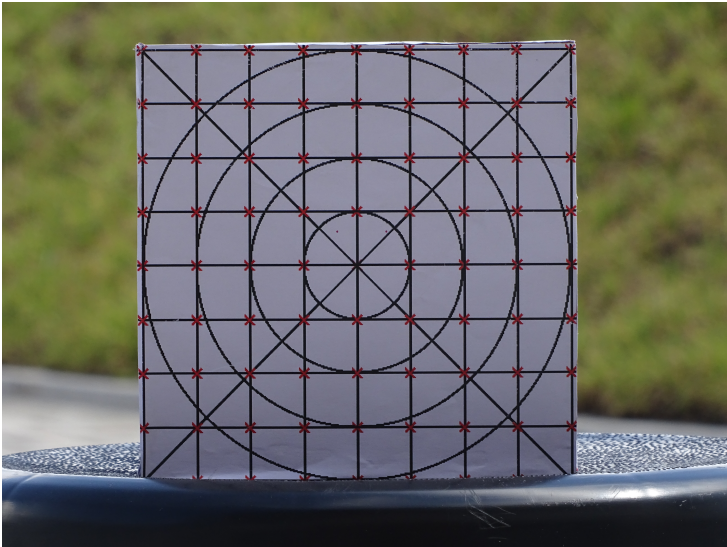


Figure 3.2: Orthophoto 1

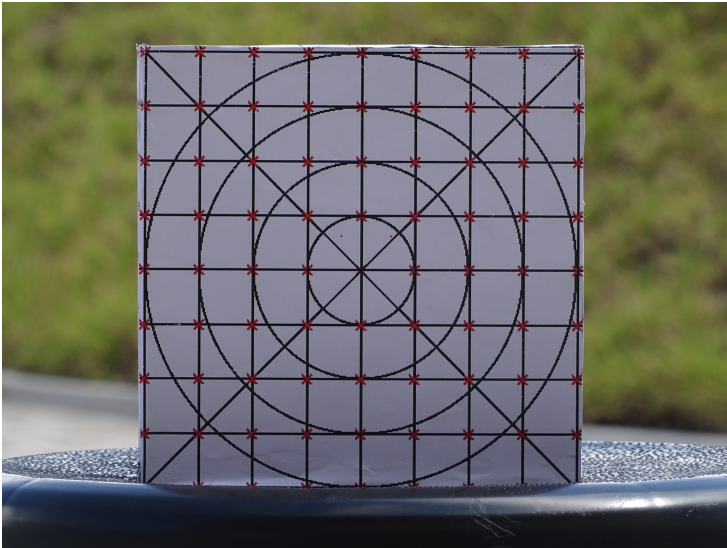


Figure 3.3: Orthophoto 2

The size in pixels of the lattice pattern on the orthophotos was measured using the measure tool of the GIMP software. Its size was 3065x3060 pixels for Orthophoto 1 and 3090x3080 for Orthophoto 2.

The multiplication factor that will be applied to the lattice pattern image in order to match its size with the orthophoto will be useful in future sections:

Orthophoto 1:

$$\begin{aligned}
K_{x1} &= \frac{\text{size in pixels of lattice in } x \text{ axis of orthophoto}}{\text{size in pixels of lattice in } x \text{ axis of image}} \\
&= \frac{3065}{397} \approx 7.720 \\
K_{y1} &= \frac{\text{size in pixels of lattice in } y \text{ axis of orthophoto}}{\text{size in pixels of lattice in } y \text{ axis of image}} \\
&= \frac{3060}{398} \approx 7.688
\end{aligned} \tag{3.3}$$

Orthophoto 2:

$$\begin{aligned}
K_{x2} &= \frac{3090}{397} \approx 7.783 \\
K_{y2} &= \frac{3080}{398} \approx 7.738
\end{aligned} \tag{3.4}$$

3.3 Feature Points Detection

In order to obtain the lens radial distortion, it is necessary to establish a correspondence among the orthophotos and the original lattice image. This is achieved by identifying a set of feature points on each orthophoto. Although there are already feature points detection algorithms such as SIFT and SURF, these algorithms do not obtain a matching rate greater than 60 % on images with lens distortions [30]. For this reason, the feature points detection was performed manually.

To manually detect feature points, the "GNU Image Manipulation Program" (GIMP) was used. A zoom was made at each of the 81 lattice feature points to accurately obtain the pixel coordinates of each distorted feature point (x_{id}, y_{id}) .

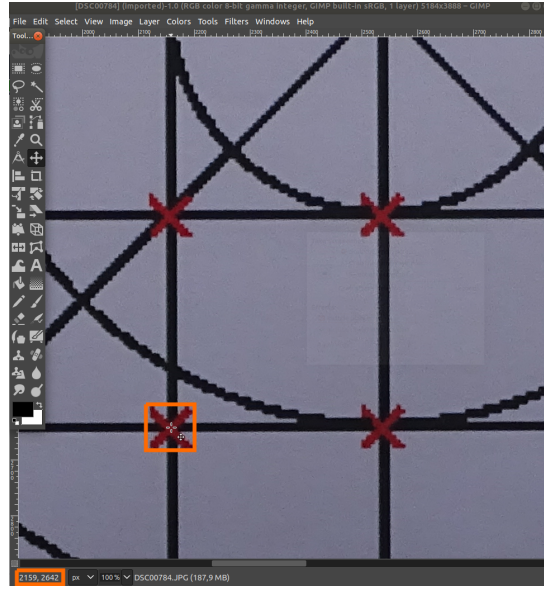


Figure 3.4: Manual Feature Points Detection using GIMP

The coordinates were used to obtain the radial distance of the distorted feature points:

$$r_{di} = \sqrt{(x_{di} - x_c)^2 + (y_{di} - y_c)^2} \quad \text{for } i = 1, \dots, 81. \quad (3.5)$$

Due to the method used for the feature detection, we can say that the data obtained have an uncertainty equal to $\sqrt{2} * \text{pixel size}$.

3.4 Radial Distortion

As detailed in (2.3), the radial distortions of the 81 feature points can be obtained by subtracting the radial distance of the undistorted feature points from the radial distance of the distorted feature points.

In order to obtain the radial distance of the undistorted feature points, the pixel coordinates of each of them are needed. These are obtained with the following equations:

$$\begin{aligned} x_{ui} &= x_c + \Delta_x * K_x \quad \text{for } i = 1, \dots, 81. \\ y_{ui} &= y_c + \Delta_y * K_y \quad \text{for } i = 1, \dots, 81. \end{aligned} \quad (3.6)$$

where: x_c and y_c are the coordinates of the center of the lattice on the image. Δ_x and Δ_y are the constant values for x and y defined in (3.1) and K_x and K_y are the multiplication factor defined in (3.4).

After the coordinates of the undistorted feature points were obtained, the radial distance of each of them was computed as before:

$$r_{ui} = \sqrt{(x_{ui} - x_c)^2 + (y_{ui} - y_c)^2} \quad \text{for } i = 1, \dots, 81. \quad (3.7)$$

Then, the radial distortion of each feature point was obtained using (2.3):

$$dr_i = r_{di} - r_{ui} \quad \text{for } i = 1, \dots, 81. \quad (3.8)$$

Finally, the lattice pattern image was overlapped on the 2 orthophotographs of the cube using GIMP to be able to optically observe the lens distortion. In order to superimposed them with the correct dimension, the multiplication factors Δ_x and Δ_y were applied to the lattice pattern image.

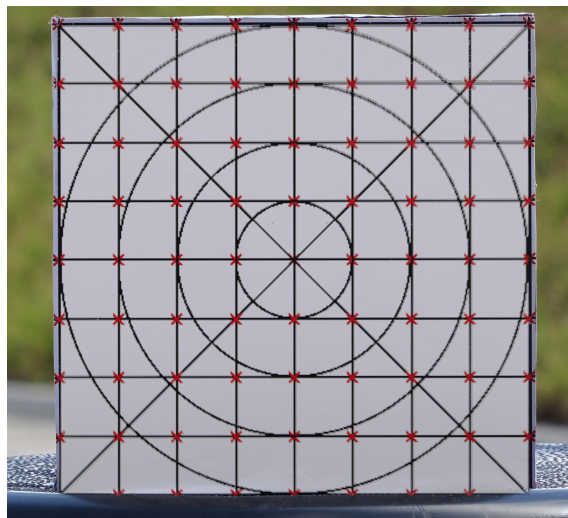


Figure 3.5: Lattice pattern image superimposed on Orthophoto 1

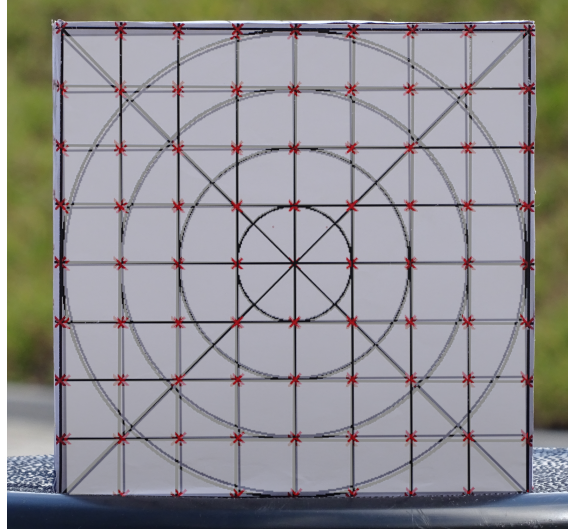


Figure 3.6: Lattice pattern image superimposed on Orthophoto 2

3.5 Experiments

The objective of the experiments is to compare the residuals of the mathematical models obtained with different data fitting methods. For this, 4 different experiments were carried out with a different number of observation points. All the data used in the Experiments were normalized in order to handle the calculus easier.

All the models are based on (2.1), but one extra term was added in the Taylor's Expansion in order to achieve a better accuracy:

$$dr = a_1r + a_2r^3 + a_3r^5 + a_4r^7 + a_5r^9 \quad (3.9)$$

3.5.1 Experiment 1: 81 Feature Points

Minimize the sum of squares of the vertical distance:

$$\begin{bmatrix} dr_1 \\ dr_2 \\ \vdots \\ dr_{80} \\ dr_{81} \end{bmatrix} = \begin{bmatrix} r_{d1} & r_{d1}^3 & r_{d1}^5 & r_{d1}^7 & r_{d1}^9 \\ r_{d2} & r_{d2}^3 & r_{d2}^5 & r_{d2}^7 & r_{d2}^9 \\ \vdots & \vdots & \vdots & \vdots & \vdots \\ r_{d80} & r_{d80}^3 & r_{d80}^5 & r_{d80}^7 & r_{d80}^9 \\ r_{d81} & r_{d81}^3 & r_{d81}^5 & r_{d81}^7 & r_{d81}^9 \end{bmatrix} \begin{bmatrix} a_1 \\ a_2 \\ a_3 \\ a_4 \\ a_5 \end{bmatrix} + \begin{bmatrix} \epsilon_1 \\ \epsilon_2 \\ \vdots \\ \epsilon_{80} \\ \epsilon_{81} \end{bmatrix}$$

or:

$$D_{[81,1]} = R_{[81,5]}A_{[5,1]} + \epsilon_{[81,1]}, \quad (3.10)$$

where: D is the normalized vector with the radial distortion of each feature point calculated with (3.8). A is the vector of distortion coefficients. R is the normalized matrix of the radial distance of each distorted feature points. And, ϵ is the residual vector.

For this model, ϵ is the difference between the observed distortion and the model distortion:

$$\epsilon = D - \hat{D}. \quad (3.11)$$

The optimization problem for this model is the following:

Find $\min_A S(A)$ for $S(A) = \sum_{i=1}^n \epsilon_i^2 = \epsilon^\top \epsilon = (D - RA)^\top (D - RA)$.

The estimation of the parameters a_1, a_2, a_3, a_4, a_5 was made as follows:

$$A = (R^\top R)^{-1} R^\top D. \quad (3.12)$$

Then, the distortion vector of the model is:

$$\hat{D} = AR. \quad (3.13)$$

Finally, the Root Mean Square Error and the L-infinity Norm were obtained as follows:

$$\begin{aligned} \text{RMSE} &= \sqrt{\frac{\epsilon^T \epsilon}{81}}, \\ \|\epsilon\|_{\infty} &= \max_i |\epsilon_i|. \end{aligned} \quad (3.14)$$

Parts of the Maxima code will be show below. ¹

Code to calculate distortion coefficients

```

`/*Code to get the Distortion Parameters Vector (A) for methods:
–Minimize the sum of squares of the vertical distance
–Minimize the sum of squares of the orthogonal distance*/'
`/*Read the R matrix normalized (Radial Distances) of the 81 Feature Points*/'
R : read_matrix("RMatrix_O1.csv")$
`/*Read the Distortion Vector of the 81 feature points*/'
D: read_matrix("DVector_O1.csv")$
Rf: col (R,5)$
RDON: addcol(Rf,D)$
RDONI : args(RDON)$
`/*Calculate the transpose of R Matrix*/'
RT: transpose(R)$
RTR: RT.R$
`/*Calculate the determinant of RT*R in order to know if the matrix is invertible .*/'
Det: determinant (RTR)$
I: invert (RTR)$
`/* Calculate the estimation parameters a1,a2,a3,a4 and a5. A=inv(RTR)*RT*D*/'
A:I.RT.D;

```

¹The complete source code is available in <https://github.com/Mafer2212/AlgebraicRadialDistortionModels>

Code to calculate epsilon, RMSE and L Infinity Norm for vertical distance method

```

`/*Epsilon for method with vertical distance*/
Epsilon1: D-Dmod$
`/* Absolute Value of Epsilon Vector*/
AbsEpsilon1: abs(Epsilon1)$
`/*RMSE and L infinity norm*/
`/*RMSE*/
SumE1: transpose(Epsilon1).Epsilon1 $
RSME1= sqrt(SumE1/81);
`/* Infinity Norm */
Epsilon1List: args(transpose(AbsEpsilon1))$
LInf1= lmax(Epsilon1List[1]);

```

Minimize the sum of squares of the orthogonal distance:

$$\begin{bmatrix} dr_1 \\ dr_2 \\ \vdots \\ dr_{80} \\ dr_{81} \end{bmatrix} = \begin{bmatrix} r_{d1} & r_{d1}^3 & r_{d1}^5 & r_{d1}^7 & r_{d1}^9 \\ r_{d2} & r_{d2}^3 & r_{d2}^5 & r_{d2}^7 & r_{d2}^9 \\ \vdots & \vdots & \vdots & \vdots & \vdots \\ r_{d80} & r_{d80}^3 & r_{d80}^5 & r_{d80}^7 & r_{d80}^9 \\ r_{d81} & r_{d81}^3 & r_{d81}^5 & r_{d81}^7 & r_{d81}^9 \end{bmatrix} \begin{bmatrix} a_1 \\ a_2 \\ a_3 \\ a_4 \\ a_5 \end{bmatrix} + \begin{bmatrix} \epsilon_1 \\ \epsilon_2 \\ \vdots \\ \epsilon_{80} \\ \epsilon_{81} \end{bmatrix}$$

or:

$$D_{[81,1]} = R_{[81,5]}A_{[5,1]} + \epsilon_{[81,1]}. \quad (3.15)$$

For this model, ϵ is the orthogonal distance from the observed point and the model, i.e.,

$$\epsilon = V \cdot \vec{N}, \quad (3.16)$$

where: V is the matrix of the difference of Distortion (ΔD) and \vec{N} is the Unitary Normal Vector.

To be more precise, we define the V matrix and the \vec{N} vector as follows:

$$V = \begin{bmatrix} 0 & 0 & 0 & 0 & 0 & \Delta D_1 \\ 0 & 0 & 0 & 0 & 0 & \Delta D_2 \\ \vdots & \vdots & \vdots & \vdots & \vdots & \vdots \\ 0 & 0 & 0 & 0 & 0 & \Delta D_{80} \\ 0 & 0 & 0 & 0 & 0 & \Delta D_{81} \end{bmatrix}, \quad (3.17)$$

$$\vec{N} = \frac{1}{\sqrt{A_1^2 + A_2^2 + A_3^2 + A_4^2 + A_5^2 + 1}} \begin{bmatrix} A_1 \\ A_2 \\ A_3 \\ A_4 \\ A_5 \\ -1 \end{bmatrix}. \quad (3.18)$$

The optimization problem for this model is the following:

$$\text{Find } \min_A S(A) \text{ for } S(A) = \sum_{i=1}^n \epsilon_i^2 = \epsilon^\top \epsilon = (V \cdot \vec{N})^\top (V \cdot \vec{N})$$

As justified above, the algebraic method that minimizes the Orthogonal distance has the same parameter estimation as the method that minimizes the vertical distance to the model, the only difference between them is the definition of its residual.

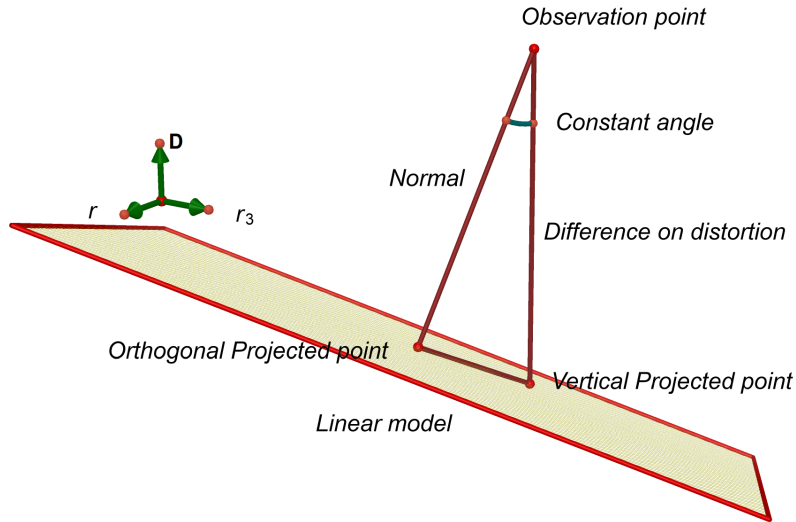


Figure 3.7: Orthogonal distance vs Vertical Distance

The parameters vector A and the distortion vector of the model \hat{D} are the same as the previous model. In this case, ΔD will be used in the computation of ϵ of this model:

$$D - \hat{D} = \Delta D. \quad (3.19)$$

Finally, the Root Mean Square Error and the L-infinity Norm were obtained as follows:

$$\begin{aligned} \text{RMSE} &= \sqrt{\frac{\epsilon^T \epsilon}{81}}, \\ \|\epsilon\|_{\infty} &= \max_i |\epsilon_i|. \end{aligned} \quad (3.20)$$

Code to calculate epsilon, RMSE and L Infinity Norm for orthogonal distance method

```

/*Epsilon for Orthogonal distance from the point to the model. d(R,H)= V*N*/
/*N vector is the Unitary Normal Vector */
n: 1/sqrt( first (A)^2+ second(A)^2+ third (A)^2+ fourth(A)^2+ fifth(A)^2+1)$
An: addrow (A, [-1])$
N: An.n$

/*V matrix is a zero matrix with the delta D values on the last column*/
v: zeromatrix(81,5)$
V: addcol(v, Epsilon1)$
Epsilon2: V.N$

/* Absolute Value of Epsilon Vector*/
AbsEpsilon2: abs(Epsilon2)$

/*RMSE and L infinity norm of Linear Non Parametric Model*/
/*RMSE*/
SumE2: transpose(Epsilon2).Epsilon2 $
RSME2= sqrt(SumE2/81);

/* L-Infinity Norm*/
Epsilon2List: args(transpose(A)

```

3.5.2 Experiment 2: 5 Greatest Feature Points in Distortion

Minimize the sum of squares of the vertical distance:

Subsequently, the 5 points with the greatest difference of distortion (ϵ) were taken because they correspond to the points with more influence in the error measure. Then, with these points, we have the following model:

$$\begin{bmatrix} dr_1 \\ dr_2 \\ dr_3 \\ dr_4 \\ dr_5 \end{bmatrix} = \begin{bmatrix} r_{d1} & r_{d1}^3 & r_{d1}^5 & r_{d1}^7 & r_{d1}^9 \\ r_{d2} & r_{d2}^3 & r_{d2}^5 & r_{d2}^7 & r_{d2}^9 \\ r_{d3} & r_{d3}^3 & r_{d3}^5 & r_{d3}^7 & r_{d3}^9 \\ r_{d4} & r_{d4}^3 & r_{d4}^5 & r_{d4}^7 & r_{d4}^9 \\ r_{d5} & r_{d5}^3 & r_{d5}^5 & r_{d5}^7 & r_{d5}^9 \end{bmatrix} \begin{bmatrix} a_1 \\ a_2 \\ a_3 \\ a_4 \\ a_5 \end{bmatrix} + \begin{bmatrix} \epsilon_1 \\ \epsilon_2 \\ \epsilon_3 \\ \epsilon_4 \\ \epsilon_5 \end{bmatrix}$$

or:

$$D_{[5,1]} = R_{[5,5]}A_{[5,1]} + \epsilon_{[5,1]}. \quad (3.21)$$

The estimation of parameters, the distortion vector, epsilon, the RMSE and L-infinity Norm of this model was obtained as in Experiment 1.

Minimize the sum of squares of the orthogonal distance:

The same 5 points with the greatest difference of distortion (ΔD) were taken in this experiment. Then, with these points we have the following model:

$$\begin{bmatrix} dr_1 \\ dr_2 \\ dr_3 \\ dr_4 \\ dr_5 \end{bmatrix} = \begin{bmatrix} r_{d1} & r_{d1}^3 & r_{d1}^5 & r_{d1}^7 & r_{d1}^9 \\ r_{d2} & r_{d2}^3 & r_{d2}^5 & r_{d2}^7 & r_{d2}^9 \\ r_{d3} & r_{d3}^3 & r_{d3}^5 & r_{d3}^7 & r_{d3}^9 \\ r_{d4} & r_{d4}^3 & r_{d4}^5 & r_{d4}^7 & r_{d4}^9 \\ r_{d5} & r_{d5}^3 & r_{d5}^5 & r_{d5}^7 & r_{d5}^9 \end{bmatrix} \begin{bmatrix} a_1 \\ a_2 \\ a_3 \\ a_4 \\ a_5 \end{bmatrix} + \begin{bmatrix} \epsilon_1 \\ \epsilon_2 \\ \epsilon_3 \\ \epsilon_4 \\ \epsilon_5 \end{bmatrix}$$

or:

$$D_{[5,1]} = R_{[5,5]}A_{[5,1]} + \epsilon_{[5,1]}. \quad (3.22)$$

The estimation of parameters, the distortion vector, epsilon, the RMSE and L-infinity Norm of this model was obtained as in Experiment 1.

Wu's Method:

With the same 5 points, we have the following system of polynomials:

$$\begin{aligned}
P_1(a_1, a_2, a_3, a_4, a_5) &= a_1 r_{d_1}^9 + a_2 r_{d_1}^7 + a_3 r_{d_1}^5 + a_4 r_{d_1}^3 + a_5 r_{d_1} - dr_1 \\
P_2(a_1, a_2, a_3, a_4, a_5) &= a_1 r_{d_2}^9 + a_2 r_{d_2}^7 + a_3 r_{d_2}^5 + a_4 r_{d_2}^3 + a_5 r_{d_2} - dr_2 \\
P_3(a_1, a_2, a_3, a_4, a_5) &= a_1 r_{d_3}^9 + a_2 r_{d_3}^7 + a_3 r_{d_3}^5 + a_4 r_{d_3}^3 + a_5 r_{d_3} - dr_3 \\
P_4(a_1, a_2, a_3, a_4, a_5) &= a_1 r_{d_4}^9 + a_2 r_{d_4}^7 + a_3 r_{d_4}^5 + a_4 r_{d_4}^3 + a_5 r_{d_4} - dr_4 \\
P_5(a_1, a_2, a_3, a_4, a_5) &= a_1 r_{d_5}^9 + a_2 r_{d_5}^7 + a_3 r_{d_5}^5 + a_4 r_{d_5}^3 + a_5 r_{d_5} - dr_4
\end{aligned} \tag{3.23}$$

After applying Wu's Polynomial Elimination Method, we have the following triangular system:

$$\begin{aligned}
P_1(a_1, a_2, a_3, a_4, a_5) &= a_1 r_{d_1}^9 + a_2 r_{d_1}^7 + a_3 r_{d_1}^5 + a_4 r_{d_1}^3 + a_5 r_{d_1} - dr_1 \\
P'_2(a_1, a_2, a_3, a_4) &= a_1 A_{11} + a_2 A_{21} + a_3 A_{31} + a_4 A_{41} + A_{01} \\
P'_3(a_1, a_2, a_3) &= a_1 A_{12} + a_2 A_{22} + a_3 A_{32} + A_{02}, \\
P'_4(a_1, a_2) &= a_1 A_{13} + a_2 A_{23} + A_{03} \\
P'_5(a_1) &= a_1 A_{14} + A_{04}
\end{aligned} \tag{3.24}$$

where the A_{ij} are formal coefficients in the r_{dk} where $k = 1 \dots 5$.

Residual

Finally, the Root Mean Square Error and the L-infinity Norm were obtained as follows:

$$\begin{aligned}
\text{RMSE} &= \sqrt{\frac{\epsilon^\top \epsilon}{81}}, \\
\|\epsilon\|_\infty &= \max_i |\epsilon_i|.
\end{aligned} \tag{3.25}$$

where:

$$\epsilon_i = \min_{(r,d) \in V(\{P_{WU, Normal}\})} \{d_E((r_i, d_i), (r, d))\} \quad \text{for } i = 1, \dots, 5. \tag{3.26}$$

Code to calculate distortion coefficients with Wu's Method

```

load(grobner);
'/* define the 5 polynomials with the points (r,d) which gives the five greatest DELTA D
for Orthophoto 1*/'
p1 : a1*(0.61615)+a3*(0.61615)^3+a5*(0.61615)^5+a7*(0.61615)^7+a9*(0.61615)^9-
      (0.0054821);
p2 : a1*(0.60924)+a3*(0.60924)^3+a5*(0.60924)^5+a7*(0.60924)^7+a9*(0.60924)^9-
      (-0.0081988);
p3 : a1*(0.71541)+a3*(0.71541)^3+a5*(0.71541)^5+a7*(0.71541)^7+a9*(0.71541)^9-
      (-0.0048082);
p4 : a1*(0.91477)+a3*(0.91477)^3+a5*(0.91477)^5+a7*(0.91477)^7+a9*(0.91477)^9-
      (-0.006484);
p5 : a1*(0.9512)+a3*(0.9512)^3+a5*(0.9512)^5+a7*(0.9512)^7+a9*(0.9512)^9- (-0.0063481);
'/* Generate the S- polynomial between 2 polynomials*/'
pr11:poly_s_polynomial(p1,p2,[a9])$
pr12:poly_s_polynomial(p1,p3,[a9])$
pr13:poly_s_polynomial(p1,p4,[a9])$
pr14:poly_s_polynomial(p1,p5,[a9])$
pr21:poly_s_polynomial(pr11,pr12,[a7])$
pr15:poly_s_polynomial(p2,p3,[a9])$
pr16:poly_s_polynomial(p2,p4,[a9])$
pr17:poly_s_polynomial(p2,p5,[a9])$
pr18:poly_s_polynomial(p3,p4,[a9])$
pr19:poly_s_polynomial(p3,p5,[a9])$
pr20:poly_s_polynomial(p4,p5,[a9])$
pr22:poly_s_polynomial(pr11,pr13,[a7])$
pr23:poly_s_polynomial(pr11,pr14,[a7])$
pr24:poly_s_polynomial(pr11,pr15,[a7])$
pr25:poly_s_polynomial(pr11,pr16,[a7])$
pr26:poly_s_polynomial(pr11,pr17,[a7])$

```

```

pr31:poly_s_polynomial(pr21,pr22,[a5])$
pr32:poly_s_polynomial(pr21,pr23,[a5])$
pr33:poly_s_polynomial(pr21,pr26,[a5])$
pr41:poly_s_polynomial(pr31,pr32,[a3])$
'/*Solving the linear equation to obtain a1*/'
l1: linsolve (pr41,a1);
pa1:l1 [1];
'/*transform the fractional answer into decimal*/'
a1: float (pa1);
'/*Solving the linear equation to obtain a3 using the value of a1 obtained before*/'
l2: linsolve (pr31,a3);
a3: ev(l2 [1], numer, expand, a1=-11.71152835355197);
'/*Solving the linear equation to obtain a5 using the value of a1 and a3 obtained before*/'
l3: linsolve (pr21,a5);
a5: ev(l3 [1], numer, expand, a1=-11.71152835355197, a3=81.11892796116398);
'/*Solving the linear equation to obtain a7 using the value of a1, a3 and a5 obtained before*/'
l4: linsolve (pr11,a7);
a7: ev(l4 [1], numer, expand, a1=-11.71152835355197, a3=81.11892796116398, a5=
-201.3149002219625);
'/*Solving the linear equation to obtain a9 using the value of a1, a3, a5, a7 and a9 obtained
before*/'
l5: linsolve (p1,a9);
a9: ev(l5 [1], numer, expand, a1=-11.71152835355197, a3=81.11892796116398, a5=
-201.3149002219625, a7= 212.3307920836902);

```

Cubic Spline Interpolation:

In order to have a more precise piecewise cubic polynomial we have added the origin

point $(0,0)$, therefore we have 6 points:

$$\begin{aligned}
 P_1 &= (r_1, d_1) = (0, 0) \\
 P_2 &= (r_2, d_2) \\
 P_3 &= (r_3, d_3) \\
 P_4 &= (r_4, d_4) \\
 P_5 &= (r_5, d_5) \\
 P_6 &= (r_6, d_6)
 \end{aligned} \tag{3.27}$$

Given the previous 6 points, we have the following piecewise cubic polynomial:

$$S(r) = \begin{cases} s_1(r) & \text{if } r_1 \leq r < r_2 \\ s_2(r) & \text{if } r_2 \leq r < r_3 \\ \vdots & \\ s_5(r) & \text{if } r_5 \leq r \leq r_6 \end{cases} . \tag{3.28}$$

The parameter estimation of each cubic spline was obtained using the function *cspline* of Maxima.

Residual

The residual of this model is calculated as follows:

$$\epsilon_i = \min_{(r,d) \in V(\{PCS, Normal\})} \{d_E((r_i, d_i), (r, d))\} \quad \text{for } i = 1, \dots, 6. \tag{3.29}$$

3.5.3 Experiment 3: Clusters

Given that there are observations whose distance from each other is less than the uncertainty, therefore insignificant, a clustering of the observations has been made. The clusters are been build as a subset of the Euclidean Minimum Spanning Tree where the edge length is less than the uncertainty. The centroids of each cluster are used on this

Experiment.

Minimize the sum of squares of the vertical distance:

Given the n centroid points, we have the following model:

$$\begin{bmatrix} dr_1 \\ dr_2 \\ \vdots \\ dr_{n-1} \\ dr_n \end{bmatrix} = \begin{bmatrix} r_{d1} & r_{d1}^3 & r_{d1}^5 & r_{d1}^7 & r_{d1}^9 \\ r_{d2} & r_{d2}^3 & r_{d2}^5 & r_{d2}^7 & r_{d2}^9 \\ \vdots & \vdots & \vdots & \vdots & \vdots \\ r_{dn-1} & r_{dn-1}^3 & r_{dn-1}^5 & r_{dn-1}^7 & r_{dn-1}^9 \\ r_{dn} & r_{dn}^3 & r_{dn}^5 & r_{dn}^7 & r_{dn}^9 \end{bmatrix} \begin{bmatrix} a_1 \\ a_2 \\ a_3 \\ a_4 \\ a_5 \end{bmatrix} + \begin{bmatrix} \epsilon_1 \\ \epsilon_2 \\ \vdots \\ \epsilon_{n-1} \\ \epsilon_n \end{bmatrix}$$

or:

$$D_{[n,1]} = R_{[n,5]}A_{[5,1]} + \epsilon_{[n,1]}. \quad (3.30)$$

For this model, ϵ is the difference between the centroid points and the model.

$$\epsilon = D - \hat{D}. \quad (3.31)$$

Therefore the estimation of the parameters a_1, a_2, a_3, a_4, a_5 was made as before:

$$\hat{A} = (R^T R)^{-1} R^T D. \quad (3.32)$$

Then, the distortion vector of the model is:

$$\hat{D} = \hat{A}R. \quad (3.33)$$

The RMSE and L-infinity Norm of this model were obtained as Experiment 1 and 2.

Minimize the sum of squares of the orthogonal distance:

$$\begin{bmatrix} dr_1 \\ dr_2 \\ \vdots \\ dr_{n-1} \\ dr_n \end{bmatrix} = \begin{bmatrix} r_{d1} & r_{d1}^3 & r_{d1}^5 & r_{d1}^7 & r_{d1}^9 \\ r_{d2} & r_{d2}^3 & r_{d2}^5 & r_{d2}^7 & r_{d2}^9 \\ \vdots & \vdots & \vdots & \vdots & \vdots \\ r_{dn-1} & r_{dn-1}^3 & r_{dn-1}^5 & r_{dn-1}^7 & r_{dn-1}^9 \\ r_{dn} & r_{dn}^3 & r_{dn}^5 & r_{dn}^7 & r_{dn}^9 \end{bmatrix} \begin{bmatrix} a_1 \\ a_2 \\ a_3 \\ a_4 \\ a_5 \end{bmatrix} + \begin{bmatrix} \epsilon_1 \\ \epsilon_2 \\ \vdots \\ \epsilon_{n-1} \\ \epsilon_n \end{bmatrix}$$

or:

$$D_{[n,1]} = R_{[n,5]}A_{[5,1]} + \epsilon_{[n,1]}. \quad (3.34)$$

For this model ϵ is the orthogonal distance from the observed point and the model.

$$\epsilon = V \cdot \vec{N}. \quad (3.35)$$

The estimation of parameters, the RMSE and L infinity Norm of this model were obtained as Experiment 1 and 2.

Cubic Spline Interpolation:

Given the n centroids we have the following piece cubic polynomial:

$$S(x) = \begin{cases} s_1(x) & \text{if } x_1 \leq x < x_2 \\ s_2(x) & \text{if } x_2 \leq x < x_3 \\ \vdots & \\ s_{n-1} & \text{if } x_{n-1} \leq x < x_n \end{cases}, \quad (3.36)$$

The parameter estimation of each cubic spline was obtained using the function *cspline* of Maxima.

Finally the residual, RMSE and L infinity Norm of this model were obtained as Experiment 1 and 2.

Code to calculate distortion coefficients of each spline with Cubic Spline Interpolation

```
load(numericalio);
load("eigen");
load(interpol);
load(grobner);
'/*Read the 55 centroids of the feature points of Orthophoto1*/'
centroids = read_matrix("Centroids.csv")$
centroidsl : args(centroids)$
'/*Sort centroids*/'
sortedcentroids : sort(centroidsl);
'/*Calculate the 54 splines using Cubic Spline Interpolation*/'
cspline(sortedcentroids, d1=0, dn=0)$
```

3.5.4 Experiment 4: Residuals of the 81 Feature Points and all the models

This experiment calculates the residuals of the 81 features points with the models obtained in the previous experiments.

Experiment 1

Given that this experiment was made with the 81 feature points, the residual and error measurements are the same as Experiment 1.

Experiment 2

Minimize the sum of squares of the vertical distance:

The distortion coefficients $A = [a_1, a_2, a_3, a_4, a_5]$ used for this computation were obtained in Experiment 2 with the 5 greatest feature points in distortion with the method

that minimizes the sum of squares of the vertical distance. The distortion vector of the model, \hat{D} , was obtained with the radial distance of the 81 feature points as follows:

$$\hat{D}_{[81,1]} =_{[5,1]} R_{[81,5]}. \quad (3.37)$$

The residual, RMSE and L-Infinity Norm of the model with the 81 feature points was obtained as follows:

$$\begin{aligned} \epsilon &= D - \hat{D} = \Delta D, \\ \text{RMSE} &= \sqrt{\frac{\epsilon^T \epsilon}{81}}, \\ \|\epsilon\|_{\infty} &= \max_i |\epsilon_i| \quad \text{for } i = 1, \dots, 81. \end{aligned} \quad (3.38)$$

Minimize the sum of squares of the orthogonal distance:

The same distortion coefficients obtained with the 5 observations with the previous method were used to calculate the residual of this model with the 81 feature points as follows:

$$\epsilon = V \cdot \vec{N}, \quad (3.39)$$

where:

V is the matrix of the difference of Distortion (ΔD)

\vec{N} is the Unitary Normal Vector

The RMSE and L-Infinity were obtained as detailed in previous experiments.

Wu's Method:

The distortion coefficients obtained with Wu's method were used to calculate the

residual of the 81 feature points with the model. The residual was calculated as follows:

$$\epsilon_i = \min_{(r,d) \in V(\{P_{WU}, Normal\})} \{d_E((r_i, y_i), (r, d))\} \quad for \quad i = 1, \dots, 81. \quad (3.40)$$

The RMSE and L-Infinity were obtained as detailed in previous experiments.

Cubic Spline Interpolation:

The distortion coefficients obtained with Cubic Spline Interpolation were used to calculate to the residual of the 81 feature points with the model. The residual was calculated as follows:

$$\epsilon_i = \min_{(r,d) \in V(\{P_{CS}, Normal\})} \{d_E((r_i, y_i), (r, d))\} \quad for \quad i = 1, \dots, 81. \quad (3.41)$$

The RMSE and L Infinity were obtained as detailed in previous experiments.

Experiment 3

The same calculations were made with the models obtained in Experiment 3.

Chapter 4

Results and Discussion

The results of each one of the experiments mentioned in Chapter 3 are presented through plots of the calibration models and tables comparing the RMSE and L-infinity norm of each model. There is a total of 8 experiments, 4 applied to each orthophoto. In this Chapter, we will refer to some algebraic methods as follows: Minimize the Vertical Distance as VDM, Minimize the Orthogonal Distance as ODM. The results are shown in the following subsections.

4.1 Experiment 1: 81 Feature Points

The results of Experiment 1 obtained with both Orthophotos are shown in this section. Tables 4.1 and 4.3 show the RMSE and L-infinity Norm of the models obtained with VDM and ODM with the 81 normalized feature points. Tables 4.2 and 4.4 show the same results in pixel in order to make them easy to interpret.

For Orthophoto 1, the maximum error of both models is approximately 9 pixels and the RMSE is approximately 3.6 pixels. Furthermore, for Orthophoto 2 the maximum error of both models is approximately 15 pixels and the RMSE is approximately 4 pixels, one sixth of the value obtained with the L-Infinity norm. The maximum error of Orthophoto 2 is twice the maximum error of Orthophoto 1 while their mean errors are very similar. This means that both models in the two orthophotos give good results on average, but

Orthophoto 2 has a larger out layer than Orthophoto 1.

It can be noticed from Figures 4.1 and 4.2 that the scale of the D axis is much bigger than the scale of the r axis, which means that the residual errors of both models appear far bigger than what they really are. Examining the actual residuals, one can conclude that these models for both Orthophotos constitute a good model in order to use them in the radial distortion correction, since the error measures are smaller than 5 pixel.

4.1.1 Orthophoto 1:

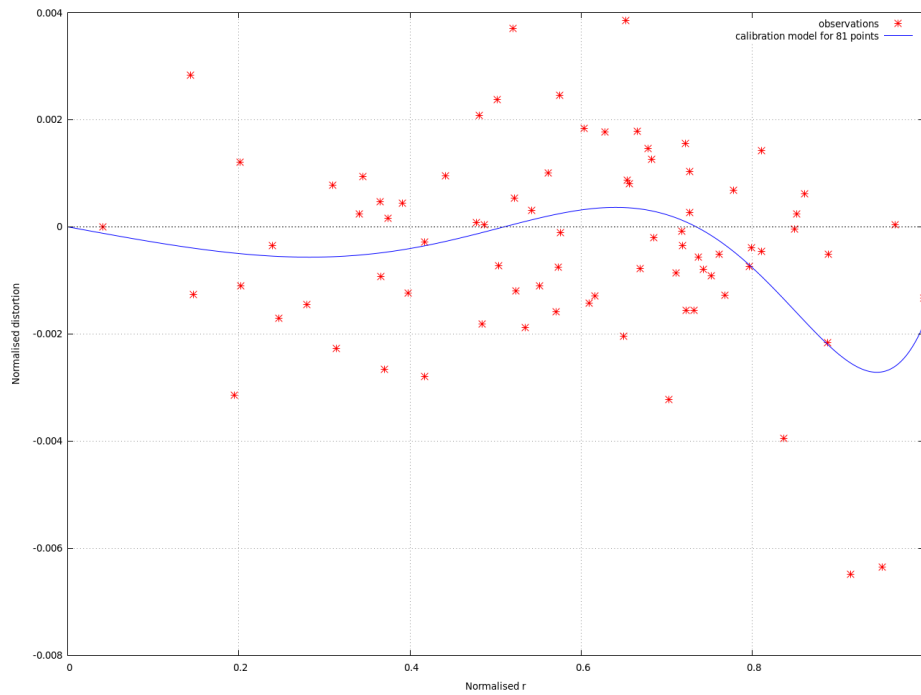


Figure 4.1: Calibration model obtained with VDM and ODM

Table 4.1: Experiment 1 - Comparison of Root Square Mean Error and L-infinity Norm of each model

Method	RMSE	L-infinity
VDM	0,00162250134262369	0,00394002288412341
ODM	0,00161197119404872	0,00391445185668038

Table 4.2: Experiment 1 - Comparison of Root Square Mean Error and L-infinity Norm of each model in pixels

Method	RMSE	L-infinity
VDM	3,65630677560249	8,87884156937211
ODM	3,63257708578879	8,82121725902924

4.1.2 Orthophoto 2

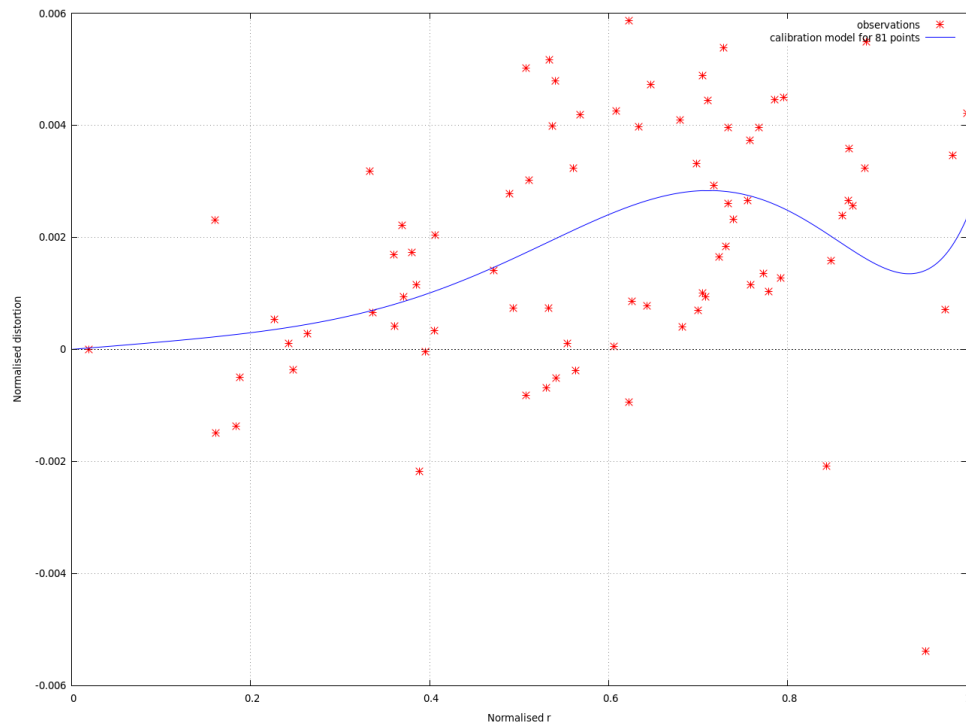


Figure 4.2: Calibration model obtained with VDM and ODM

Table 4.3: Experiment 1 - Comparison of Root Square Mean Error and L-infinity Norm of each model

Method	RMSE	L-infinity
VDM	0,00192301065285817	0,00680300547667035
ODM	0,00190692861178089	0,00674611228506883

Table 4.4: Experiment 1 - Comparison of Root Square Mean Error and L-infinity Norm of each model in pixels

Method	RMSE	L-infinity
VDM	4,28892911928263000	15,17287917472740000
ODM	4,25306102142716000	15,04598915163470000

4.2 Experiment 2: 5 Greatest Distortion Feature Points

The results of Experiment 2 obtained with both Orthophotos are shown in this section. Tables 4.5 and 4.7 show the normalized RMSE and L-infinity of the models applying VDM, ODM, Cubic Splines Interpolation, and Single Algebraic Curve using Wu's Method for the 5 Greatest Points in Distortion of both orthophotos. Tables 4.7 and 4.8 show the same results in pixels in order to make them easy to interpret.

It is clear that for Orthophoto 1 all the methods gives excellent models given that its maximum errors are 0 pixels but with different precision. However, the algebraic curve obtained with Wu's polynomial elimination gives the best model being that its maximum error is approximately $2,35E-11$ pixels, closer to zero. The same behaviour is shown for Orthophoto 2.

For Orthophoto 1, Figures 4.3 to Figure 4.5 do not show great difference between each model. The plot of the model obtained with VDM/ODM and Wu are graphically the same, however the difference in residuals is noticeable since the precision of Wu is different by 8 decimals. For Orthophoto 2, the behaviour is the same adding that the model obtained with Cubic Spline interpolation, Figure 4.7, has a prominent spike. The possible reason for this spike will be explained in the next section.

4.2.1 Orthophoto 1:

Table 4.5: Experiment 2 : 5 Greatest Feature Points in Distortion - Comparison of Root Square Mean Error and L-infinity Norm.

Method	RMSE	L-infinity
VDM	2,34511998350156E-07	3,17626752506343E-07
ODM	1,77064958702815E-07	2,39819575165065E-07
Cubic Spline	8,36335606314196E-13	1,72928833864612E-12
Wu's Elimination	8,43874796172484E-16	1,04474468442891E-15

Table 4.6: Experiment 2 : 5 Greatest Feature Points in Distortion - Comparison of Root Square Mean Error and L-infinity Norm in pixels

Method	RMSE	L-infinity
VDM	0,000528472788282	0,0007157718867730
ODM	0,000399015884437	0,0005404334126345
Cubic Spline	0,000000001884682	0,0000000038969513
Wu's Elimination	0,00000000001902	0,000000000023543

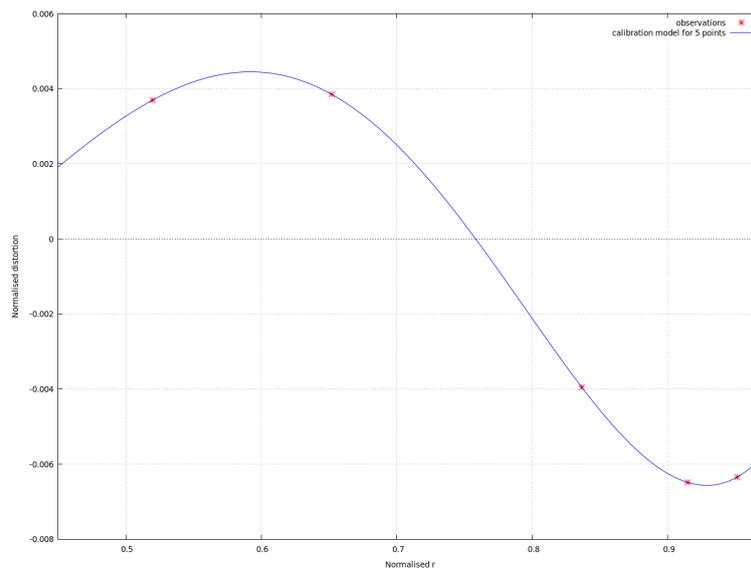


Figure 4.3: Calibration model obtained with VDM and ODM

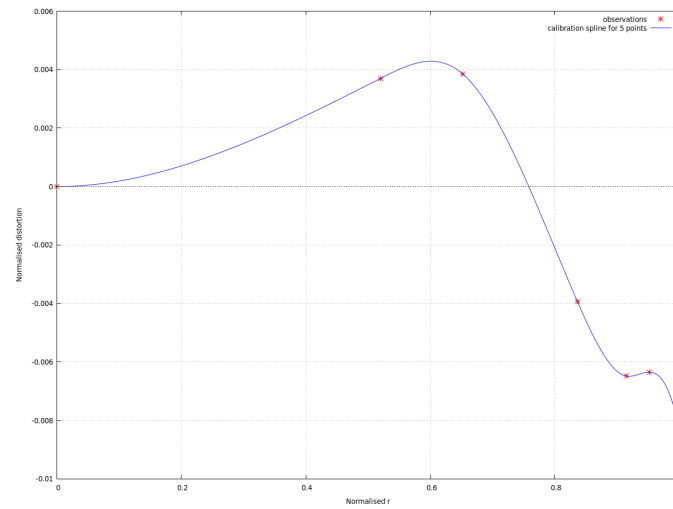


Figure 4.4: Calibration model obtained with Cubic Spline Method

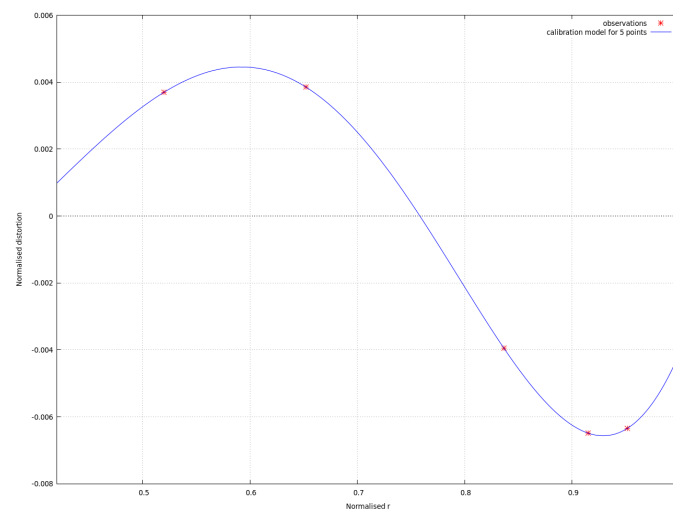


Figure 4.5: Calibration model obtained with Wu's Method

4.2.2 Orthophoto 2

Table 4.7: Experiment 2 : 5 Greatest in Distortion Feature Points - Comparison of Root Square Mean Error and L-infinity Norm.

Method	RMSE	L-infinity
VDM	4,98537144583741E-08	6,63604094132061E-08
ODM	1,56732828057551E-08	2,08627476435543E-08
Cubic splines	3,70651484494395E-11	6,10284053730989E-11
Wu's Elimination	3,66122988837112E-14	7,55307710526317E-14

Table 4.8: Experiment 2 : 5 Greatest in Distortion Feature Points - Comparison of Root Square Mean Error and L-infinity Norm in pixels

Method	RMSE	L-infinity
VDM	0,00011118973643080	0,00014800494832246
ODM	0,00003495643610733	0,00004653060332437
Cspline	0,00000008266714189	0,00000013611287307
Wu's Elimination	0,0000000008165714	0,00000000016845779

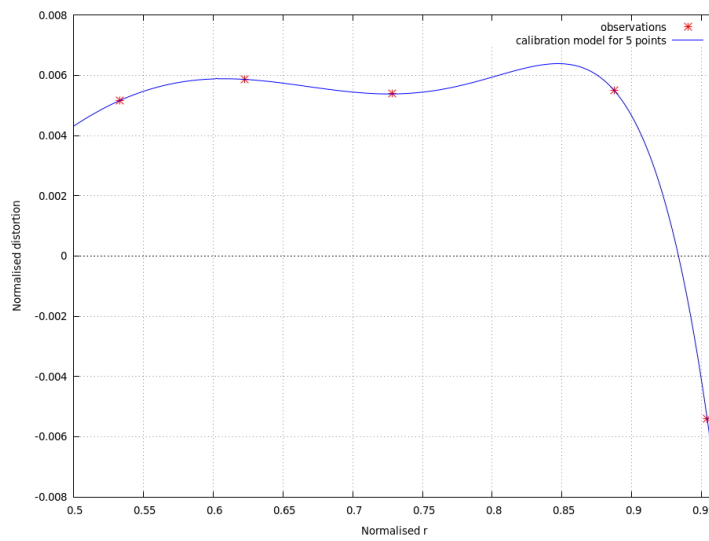


Figure 4.6: Calibration model obtained with VDM and ODM

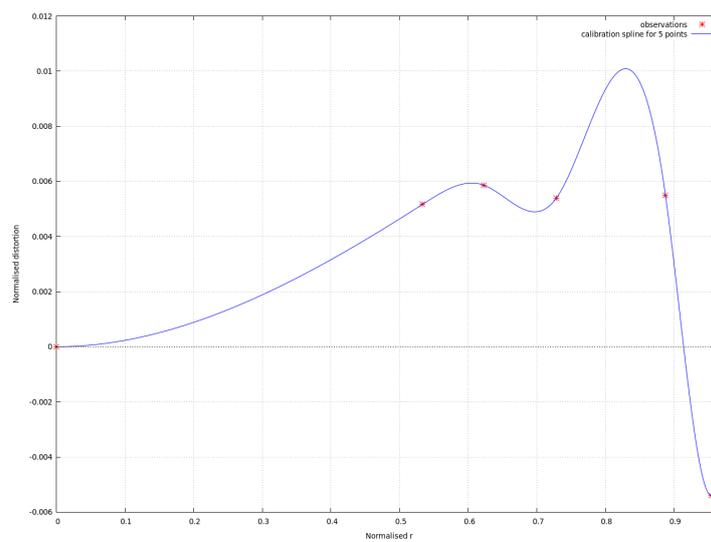


Figure 4.7: Calibration model obtained with Cubic Spline Method

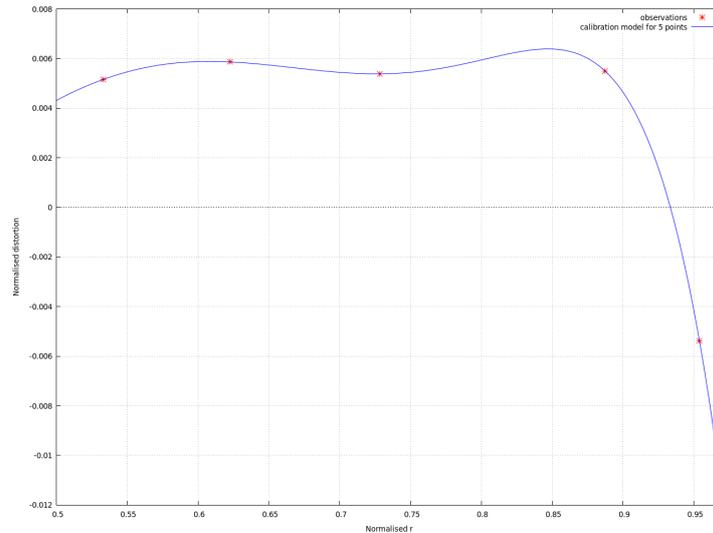


Figure 4.8: Calibration model obtained with Wu's Method

4.3 Experiment 3: Clusters

The results of Experiment 3 obtained with both Orthophotos are shown in this section. Tables 4.9 and 4.11 show the RMSE and L-infinity Norm of the models obtained applying VDM, ODM and Cubic Spline Interpolation to the centroids of the clusters obtained for each Orthophoto with the normalized data. Tables 4.10 and 4.12 show the same results in pixels in order to make them easy to interpret.

For Orthophoto 1, the maximum error and RMSE of the models obtained with VDM and ODM are almost equal to the values obtained in Experiment 1 which values are 3 and 9 pixels, respectively. However, the RMSE and the maximum error obtained with Cubic Spline interpolation are 0.06 and 0.43 pixels which indicates that this model is better than the others, therefore it is the best method for the radial distortion correction with this amount of data. The same behaviour is shown for Orthophoto 2.

It can be notice from Figure 4.10 and 4.12 show that cubic spline interpolation method suffer from the very loose control of the interpolated curves. Frequently the size and shape of these features such as spikes or sharp corners are controlled by control polygons and these polygons depend on the configuration of the initial tangent vectors of each node [31]. Therefore, the Maxima implementation of the *cspline* function may be the cause of

these spikes. Unfortunately it is not possible to access the code of this function to observe the configuration of the control polygons. The same behavior is observed for Orthophoto 2.

4.3.1 Orthophoto 1

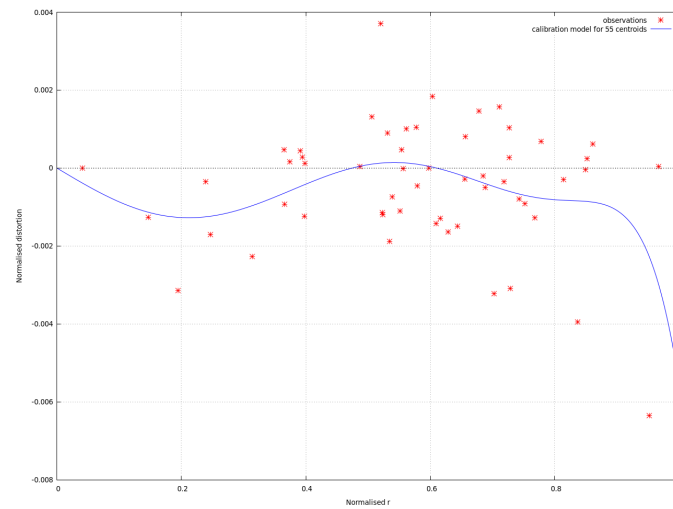


Figure 4.9: Calibration model obtained with VDM and ODM

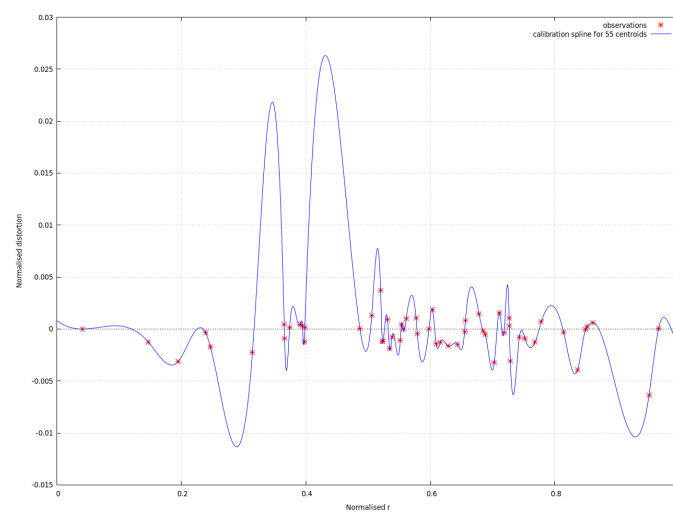


Figure 4.10: Calibration model obtained with Cubic Spline Method

Table 4.9: Experiment 3 : Cluster - Comparison of Root Square Mean Error and L-infinity Norm.

Method	RMSE	L-infinity
VDM	0,00145610179873744	0,00408925976689172
ODM	0,00129592646602684	0,00363942958038284
Cubic Spline	2,80927001949541E-05	1,93605065169300E-04

Table 4.10: Experiment 3 : Cluster - Comparison of Root Square Mean Error and L-infinity Norm in pixels.

Method	RMSE	L-infinity
VDM	3,28132540345482000	9,21514688469049000
ODM	2,92037029119148000	8,20145455939273000
Cubic Spline	0,06330689988932910	0,43628901435901800

4.3.2 Orthophoto 2

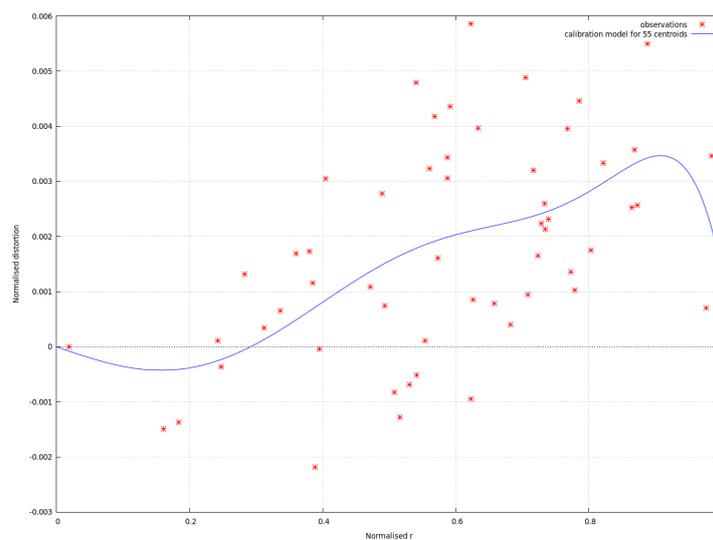


Figure 4.11: Calibration model obtained with VDM and ODM

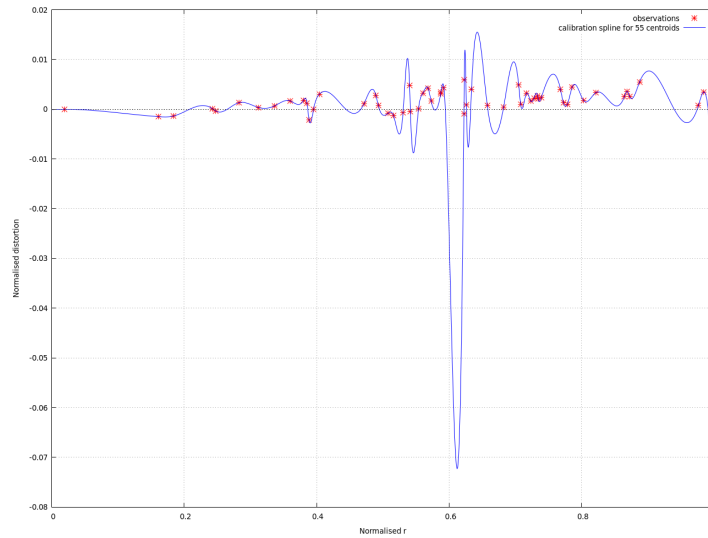


Figure 4.12: Calibration model obtained with Cubic Spline Method

Table 4.11: Experiment 3 : Cluster - Comparison of Root Square Mean Error and L-infinity Norm.

Method	RMSE	L-infinity
VDM	0,00160450071258876	0,0037615829950519
ODM	0,00151740373669321	0,0035573933048394
Cubic Spline	4,34622217606314E-04	7,34450667123198E-04

Table 4.12: Experiment 3 : Cluster - Comparison of Root Square Mean Error and L-infinity Norm in pixels.

Method	RMSE	L-infinity
VDM	3,57855002930096	8,38953378552415
ODM	3,3842959020216	7,9341254356495
Cubic Spline	0,969346624371714	1,63806001189821

4.4 Experiment 4: 81 Feature Points VS all the models

In this section, we will describe the residuals between the 81 feature points and the models obtained in the previous experiments.

4.4.1 Orthophoto 1 - Models obtained with 5 observations VS 81 observations

In this subsection, the residuals between the 81 feature points and the models obtained with the 5 Greatest Points in Distortion for Orthophoto 1 are being discussed.

For Orthophoto 1, Table 4.14 shows that the model obtained with ODM gives the best fit for the 81 Feature Points given that the RMSE and L-infinity Error are 5 pixels and 10 pixels respectively. However, all the other models gives similar error values. As a conclusion none of these models can be used for the radial distortion calibration since their RMSE and L-infinity values are very high.

As expected, the models obtained with VDM and ODM using the 81 points, (Experiment 1), give lower values of RMSE and L-infinity. However, the difference in error between these models and those obtained with the 5 greatest points is 2 to 4 pixels in the RMSE and L-infinity, so it can be said that despite having calculated the models with a very reduced amount of points, their error differences are not as significant. Graphically the difference between the models obtained in Experiment 1 and Experiment 2 is significant.

Table 4.13: Experiment 4 : 81 Feature Points VS the models with 5 points - Comparison of Root Square Mean Error and L-infinity Norm.

Method	RMSE	L-infinity
VDM	0,00317321736178327	0,0059635671834
ODM	0,00239589276912081	0,00450270683152934
Cspline	0,00335154131771229	0,00709700292933852
Wu's Elimination	0,00317541481926291	0,00596483815599785

Table 4.14: Experiment 4 : 81 Feature Points VS the models with 5 points - Comparison of Root Square Mean Error and L-infinity Norm in pixels.

Method	RMSE	L-infinity
VDM	7,1508453247786	13,4388986477494
ODM	5,39914435521375	10,1468498448514
Cspline	7,55269835946465	15,9930961012644
Wu's Elimination	7,15579729520897	13,4417627845412

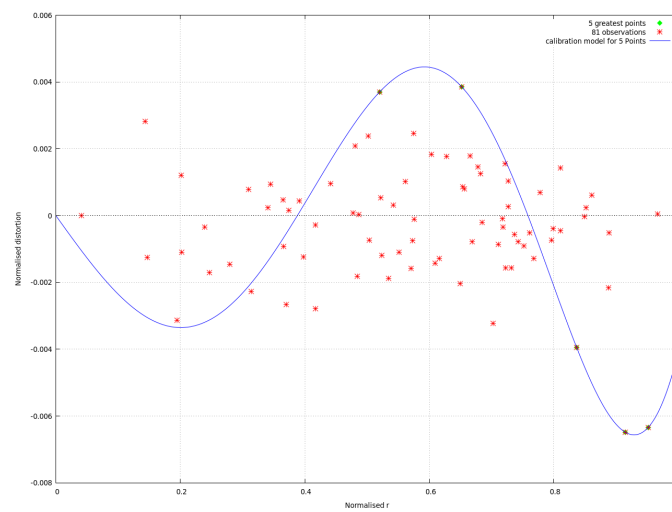


Figure 4.13: Calibration model obtained with 5 points with VDM and ODM VS 81 feature points

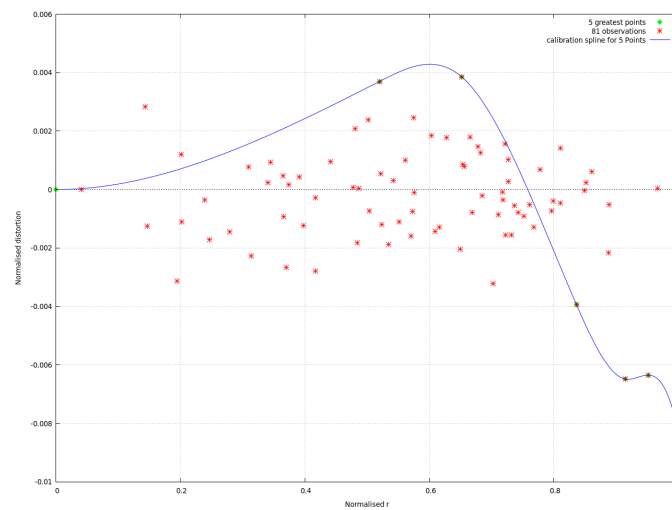


Figure 4.14: Calibration model obtained with 5 points with Cubic Spline VS 81 feature points

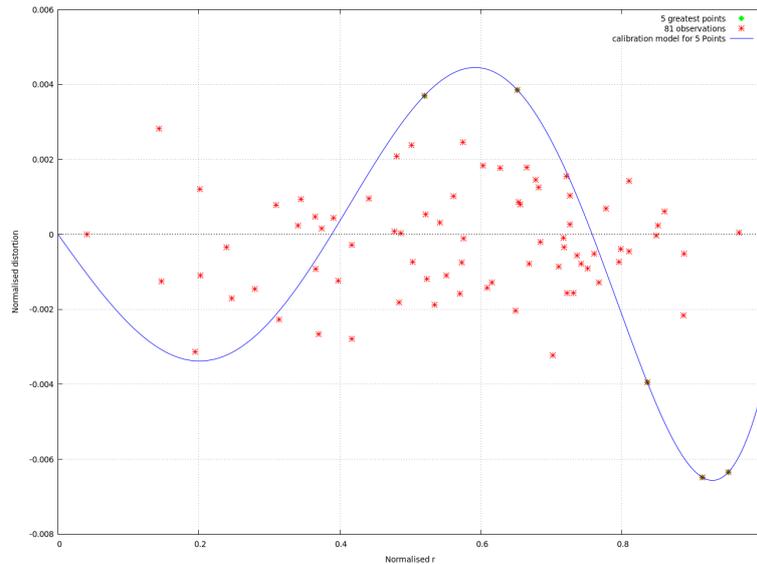


Figure 4.15: Calibration model obtained with 5 points with Wu VS 81 feature points

4.4.2 Orthophoto 2 - Models obtained with 5 observations VS 81 observations

In this subsection, the residuals between the 81 feature points and the models obtained with the 5 Greatest Points in Distortion for Orthophoto 2 are being discussed.

For Orthophoto 2, Table 4.16 shows that the model obtained with ODM gives the best fit for the 81 feature points. Unlike the observed in the previous experiments, the distinctness in error with the VDM and ODM models is very significant. It is also notorious that the RMSE and L-infinity of the other models are very high so none of these models can be used for the radial distortion calibration. Apparently Orthophoto 2 has higher outlayers than Orthophoto 1.

As expected, the models obtained with VDM and ODM using the 81 points, (Experiment 1), give lower values of RMSE and L-infinity. Graphically the difference between the models obtained in Experiment 1 and Experiment 2 is noticeable.

Table 4.15: Experiment 4 : 81 Feature Points VS the models with 5 points - Comparison of Root Square Mean Error and L-infinity Norm.

Method	RMSE	L-infinity
VDM	0,00607650877810264	0,0334526609422366
ODM	0,00191036598948663	0,0105170300999435
Cspline	0,0040056523695532	0,0119761208831621
Wu's Elimination	0,00554052714124905	0,0277882149377483

Table 4.16: Experiment 4 : 81 Feature Points VS the models with 5 points - Comparison of Root Square Mean Error and L-infinity Norm in pixels.

Method	RMSE	L-infinity
VDM	13,5525590579779	74,6101387526892
ODM	4,26072747367182	23,456342572506
Cspline	8,93388659286189	26,7105819281341
Wu's Elimination	12,3571484936706	61,97661153995880000

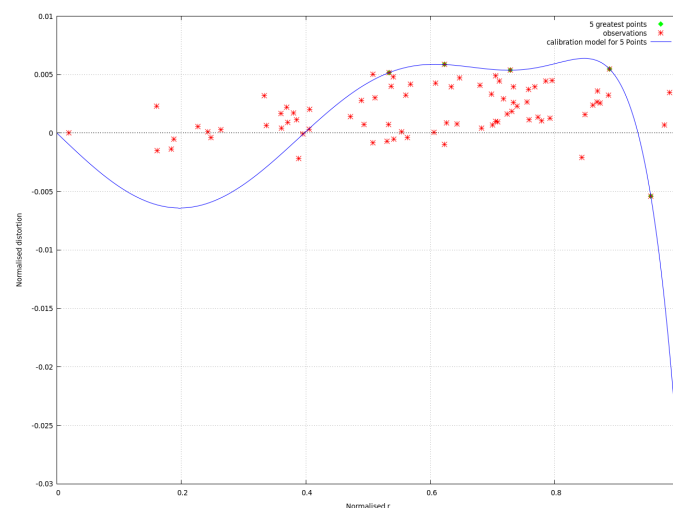


Figure 4.16: Calibration model obtained with 5 points with VDM and ODM VS 81 feature points

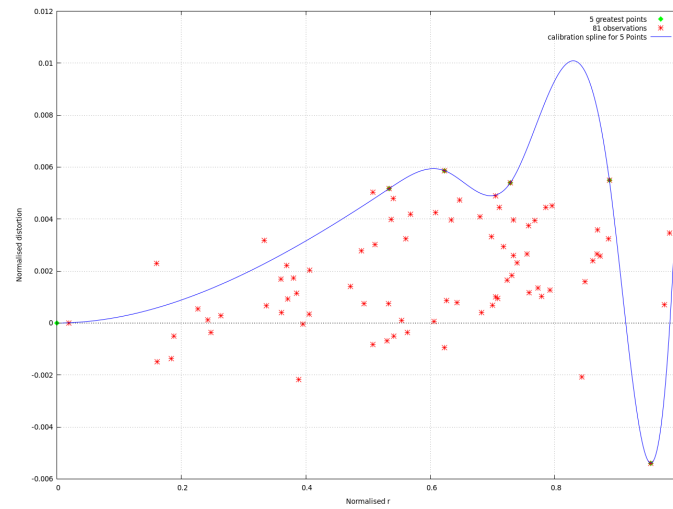


Figure 4.17: Calibration model obtained with 5 points with Cubic Spline VS 81 feature points

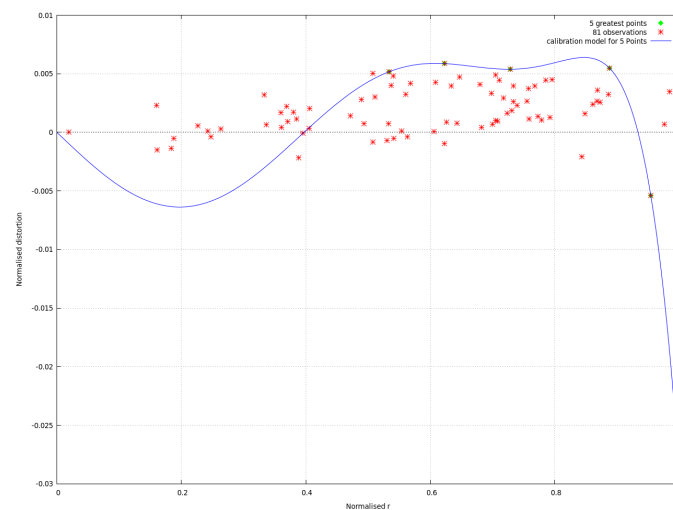


Figure 4.18: Calibration model obtained with 5 points with Wu VS 81 feature points

4.4.3 Orthophoto 1 -Models obtained with 55 centroids VS 81 observations

In this subsection, the residuals between the 81 feature points and the models obtained with the 55 centroids of the clusters of both Orthophotos are being discussed.

For Orthophoto 1, Table 4.18 shows that the model obtained with VDM and ODM gives the best fit for the 81 feature points whereas the model obtained with cubic spline

is the worst being that the RMSE and L-infinity are 15 and 63 pixels, respectively. This is given because of the lack of control that cubic spline has over the spikes as explained in Experiment 3. As seen in Figure 4.20 these spikes generate very large orthogonal distances from the feature points to the algebraic curve.

When comparing these results with those obtained in Experiment 1, we can see that the RMSE and L-infinity values of the model obtained with VDM/ODM are practically similar, so we were able to obtain models with RMSE of approximately 3 pixels with a reduced number of points, which guarantees us less calculations. Graphically the difference between the models obtained in Experiment 1 and Experiment 3 is not very significant.

The same behavior is shown for Orthophoto 2, but with much lower values of RMSE and L-Infinity for the model obtained with cubic spline than in Orthophoto 1. This is because its spikes are less prominent.

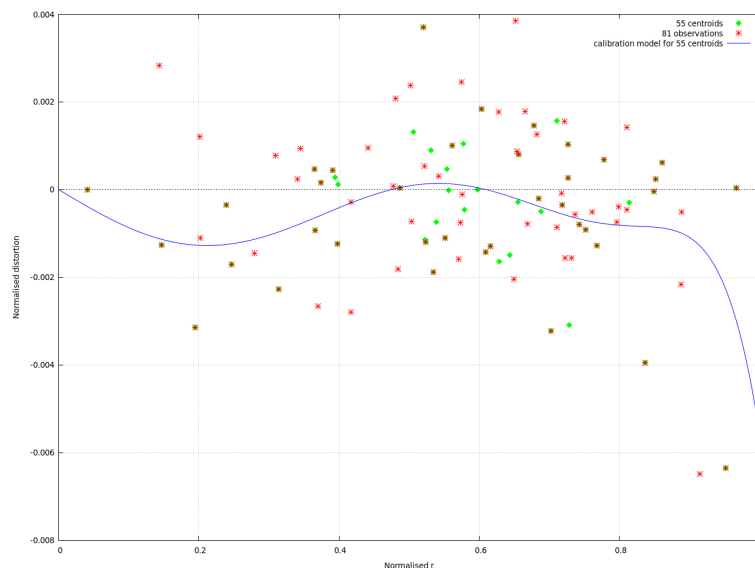


Figure 4.19: Calibration model obtained with 55 centroids with VDM and ODM VS 81 feature points

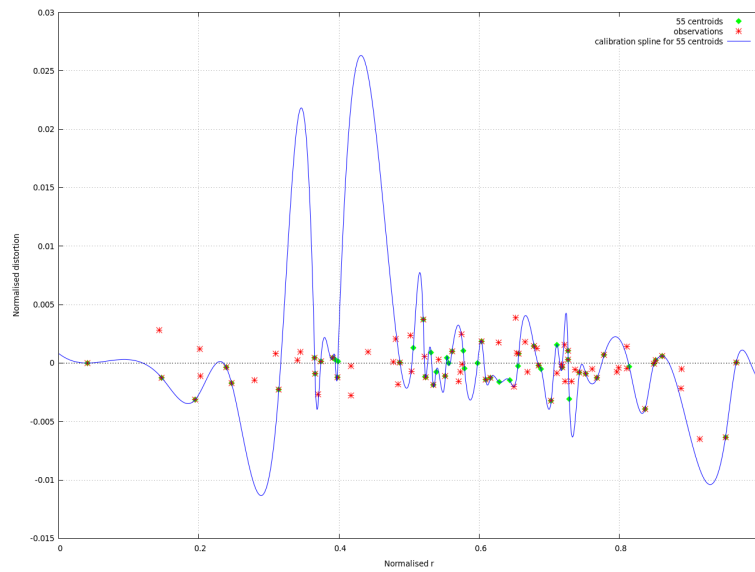


Figure 4.20: Calibration model obtained with 55 centroids with Cubic Spline VS 81 feature points

Table 4.17: Experiment 4 : 81 Feature Points VS the models with 55 centroids - Comparison of Root Square Mean Error and L-infinity Norm.

Method	RMSE	L-infinity
VDM	0,00175262148447056	0,00519967550268258
ODM	0,00155982814431107	0,00462769643202177
Cspline	0,00690145832773324	0,0277858275611668

Table 4.18: Experiment 4 : 81 Feature Points VS the models with 55 centroids - Comparison of Root Square Mean Error and L-infinity Norm in pixels.

Method	RMSE	L-infinity
VDM	3,94953251525441	11,7174687452952
ODM	3,515072723205	10,4285139095611
Cspline	15,5524363415469	62,6153624090894

4.4.4 Orthophoto 2 - Models obtained with 55 centroids VS 81 observations

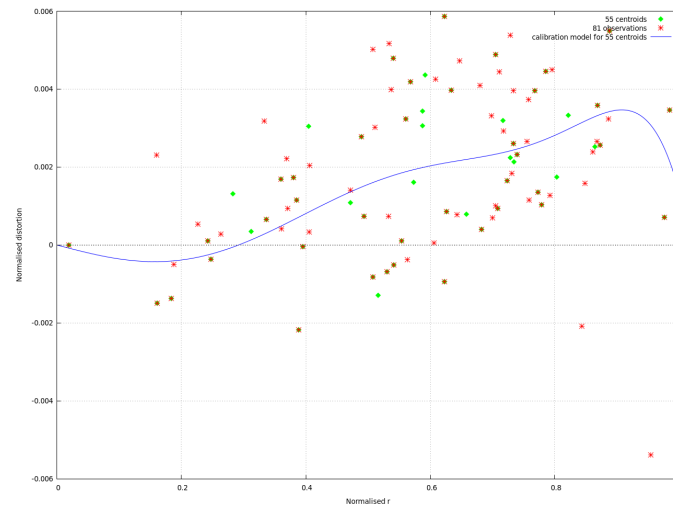


Figure 4.21: Calibration model obtained with 55 centroids with VDM and ODM VS 81 feature points

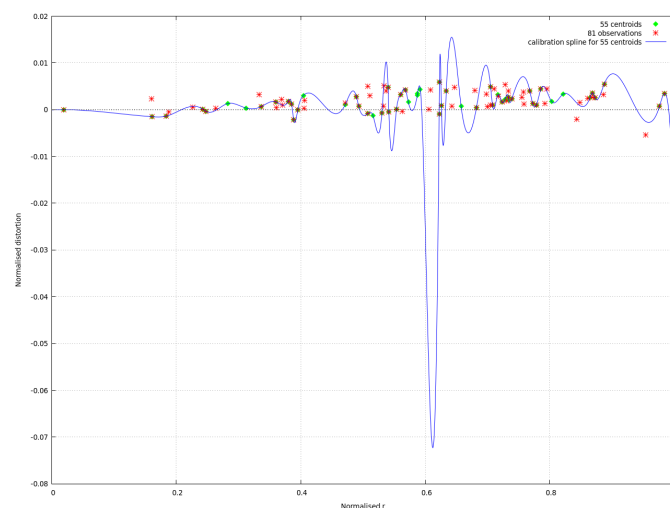


Figure 4.22: Calibration model obtained with 55 centroids with Cubic Spline VS 81 feature points

Table 4.19: Experiment 4 : 81 Feature Points VS the models with 55 centroids - Comparison of Root Square Mean Error and L-infinity Norm.

Method	RMSE	L-infinity
VDM	0,00202452640969937	0,00846576993982556
ODM	0,00191462921456444	0,00800622326926245
Cubic spline	0,0032846492007512	0,0162801747320613

Table 4.20: Experiment 4 : 81 Feature Points VS the models with 55 centroids - Comparison of Root Square Mean Error and L-infinity Norm in pixels.

Method	RMSE	L-infinity
VDM	4,5153417420807	18,8813760121917
ODM	4,27023582982736	17,8564398819014
Cubic Spline	7,32581880541942	36,309999308411

Chapter 5

Conclusions and future work

In general terms, the main goal of this research is to provide a comparative analysis of the radial distortion calibration using different algebraic methods. At a specific level, the following conclusions are specified:

- The set of feature points of the lattice transform this process into a fully deterministic radial distortion correction given that these feature point were determine without the use of non-deterministic algorithm and it was based on the manual detection of the precise pixel
- The best model was produced in the only experiment in which Wu's Method was used to obtain one algebraic curve for the 5 Greatest Feature Points. This means that Wu' is the best interpolation method for a small amount of data. However, the lineal methods VDM and ODM always gave very good models for each experiment.
- Cubic Spline is a very good interpolation method but when we try to fit the model with a bigger set of data the result are not good enough to used it for the radial distortion calibration due to little control over spikes.
- Clustering is a good way to reduce the feature point data set in order to make the data fitting calculations shorter and easy. The models and residuals obtained with clustering are almost the same that the ones obtained with 81 features points.

- We are currently working on a new experiment in which the piecewise linear curve obtained with Cubic Spline is simplified using Douglas–Peucker algorithm.

As future work, it would be advisable to apply the same experiments with a feature detection algorithm such as the Sobel filter to obtain the features points and then, apply a line search on the features in order to be able to find the lines and their intersections. This would make the Feature Detection process a little bit faster than doing it manually and would give better result than feature detection algorithms like SIFT and SURF. It would also be advisable to implement the cubic spline code in such a way that it can manipulate the splines using restrictions on the tangents of each side of the nodes, as mentioned in this work [31], so a better manipulation of the control polygons can be achieved therefore it would be possible to reduce the spikes of this algebraic curve.

References

- [1] “Colour - vertical (full frame) - photo size 10 x 10 inch, the survey and mapping office (smo) of the lands department, the government of the hong kong special administrative region,” <https://images.app.goo.gl/Ub1GwNVJFZHFMM8W6>, accessed: 2020-01-14.
- [2] J. Cartensen, *Image analysis, vision, and computer graphics*. Kongens Lyngby - Technical University of Denmark, 2002. [Online]. Available: https://www.researchgate.net/publication/269694411_Image_analysis_vision_and_computer_graphics
- [3] Y. Li, J. Zhang, W. Hu, and J. Tian, “Laboratory calibration of star sensor with installation error using a nonlinear distortion model,” *Applied Physics B: Lasers and Optics*, vol. 115, pp. 561–570, 2014.
- [4] F. Remondino and C. Fraser, “Digital camera calibration methods: Considerations and comparisons,” *Ine. Arch. Photogram. Remote Sens. Spat. Inf. Sci*, vol. 36, no. 11, 2005.
- [5] F. Zhou, Y. Cui, H. Gao, and Y. Wang, “Lined-based camera calibration with lens distortion correction from a single image,” *Optics and Lasers in Engineering*, vol. 51, pp. 1332–1343, 2013.
- [6] P. Ranganathan, “Non-parametric models of distortion in imaging systems.” 2016.
- [7] C. Mcglone, “Manual of photogrammetry,” vol. 79, 05 2013.

- [8] D. G. Lowe, "Object recognition from local scale-invariant features," in *Proceedings of the International Conference on Computer Vision-Volume 2 - Volume 2*, ser. ICCV '99. USA: IEEE Computer Society, 1999, p. 1150.
- [9] H. Bay, A. Ess, T. Tuytelaars, and L. Van Gool, "Speeded-up robust features (surf)," *Comput. Vis. Image Underst.*, vol. 110, no. 3, p. 346–359, Jun. 2008. [Online]. Available: <https://doi.org/10.1016/j.cviu.2007.09.014>
- [10] H.-G. Maas and U. Hampel, "Photogrammetric techniques in civil engineering material testing and structure monitoring," *Photogrammetric Engineering Remote Sensing*, vol. 72, pp. 39–45, 01 2006.
- [11] M. Shashi and K. Jain, "Use of photogrammetry in 3d modeling and visualization of buildings," vol. 2, 01 2007.
- [12] B. Hoogeboom, I. Alberink, and D. Vrijdag, *Photogrammetry in Digital Forensics*, 12 2015, pp. 183–218.
- [13] N. Jayaratne, J. Lo, R. Zwahlen, and L. PhD, "Three-dimensional photogrammetry for surgical planning of tissue expansion in hemifacial microsomia," *Head Neck*, vol. 32, pp. 1728 – 1735, 12 2010.
- [14] N. Shankar, R. Duraichelvan, C. Ateequlla, A. Nayak, A. Krishnan, M. Yogi, C. K. Rao, K. Vidyasagar, R. Jain, P. Mathur, K. Govinda, R. Rajeev, and T. Danabalan, "Photogrammetric measurements of a 12-metre preloaded parabolic dish antenna," 05 2009.
- [15] P. Benduch and A. Peska-Siwik, "Assessing the usefulness of the photogrammetric method in the process of capturing data on parcel boundaries," *Geodesy and Cartography*, vol. 66, pp. 3–22, 06 2017.
- [16] M. Gasparovic and D. Gajski, "Unmanned aerial photogrammetric systems in the service of engineering geodesy," 05 2016.

- [17] T. Nuttens, P. De Maeyer, A. Wulf, R. Goossens, and C. Stal, “Terrestrial laser scanning and digital photogrammetry for cultural heritage: an accuracy assessment,” 05 2011, p. 10.
- [18] J. Barnfather, M. Goodfellow, and T. Abram, “Photogrammetric measurement process capability for metrology assisted robotic machining,” *Measurement: Journal of the International Measurement Confederation*, vol. 78, pp. 29–41, 01 2016.
- [19] H. Jeong, H. Ahn, and C. Choi, “Smart camera calibration for photogrammetry application,” *35th Asian Conference on Remote Sensing 2014, ACRS 2014: Sensing for Reintegration of Societies*, 01 2014.
- [20] J. Jedlička and M. Potuckova, “Correction of radial distortion in digital images,” 01 2007.
- [21] H. Sun, *Lens Design: a practical Guide*. CRC Press, 2017. [Online]. Available: <https://books.google.com.ec/books?id=gSoNDgAAQBAJ&pg=PA86&lpg=PA86&dq=lens+design+a+practical+guide+haiyin+sun+pdf&source=bl&ots=pQGI3tY0Wa&sig=ACfU3U3c1uamDJivJ5Dp4Xtsmp0K5gsntg&hl=es&sa=X&ved=2ahUKEwiRs476sYjnAhWk1FkKHThcAwwQ6AEwCXoECAoQAQ#v=onepage&q=lens%20design%20a%20practical%20guide%20haiyin%20sun%20pdf&f=false>
- [22] A. Jadhav and S. Rurdrawar, “Review of mathematical modelling,” in *13th International Conference on Recent Innovations in Science, Engineering and Management 2018*. India: IJARSE, 2018, pp. 746–748.
- [23] Massachusetts Institute of Technology, “Maxima computer algebra system.” [Online]. Available: <http://maxima.sourceforge.net/docs/manual/maxima.html>
- [24] S. Mckinley and M. Levine, “Cubic spline interpolation.”

-
- [25] A. Philippe and M. Moreno, “Triangular sets for solving polynomial systems: a comparative implementation of four methods,” *Journal of Symbolic Computation*, vol. 28, pp. 125–154, 1999.
- [26] D. Levy, “Introduction to numerical analysis,” 2010, lecture Notes.
- [27] J. Sanchez, “Polinomios ortogonales,” 2013, lecture Notes.
- [28] I. Mugume, C. Basalirwa, D. Waiswa, J. Reuder, M. Mesquita, S. Tao, and T. Ngailo, “Comparison of parametric and nonparametric methods for analyzing the bias of a numerical model,” *Modelling and Simulation in Engineering*, vol. 2016, 05 2016.
- [29] R. Van de Geijin, “Notes on vector and matrix norms,” 2014, lecture Notes.
- [30] E. Karami, S. Prasad, and M. Shehata, “Image matching using sift, surf, brief and orb: Performance comparison for distorted images,” 2015 2015, pp. 125–154.
- [31] A. Toledo, S. Behar, W. Morales, and J. Estrada, “Manipulacion de a-splines cubicos basadas en restricciones,” *Investigación Operacional*, vol. 37, pp. 1–12, 2015.
- [32] C. Pinter, *A book of Abstract Algebra*. McGraw Hill Publishing Company, 1990.
- [33] D. Cox, J. Little, and D. OShea, *Ideals, Varieties, and Algorithms*. Springer, 2007.

Appendix A

Extra Definitions

The following definitions are based on Charles C. Pinter's Abstract Algebra Book. For more detailed definitions see [32].

A.1 Rings

By a ring we mean a set A with two binary operations called addition and multiplication which satisfies the following axioms:

- A with addition alone is an Abelian group.
- The multiplication is associative.
- The multiplication is distributive over the addition. That is, for all a, b and c in A ,

$$a(b + c) = ab + ac \tag{A.1}$$

and

$$(b + c)a = ba + ca \tag{A.2}$$

The easiest examples of rings come from the traditional number system. The set \mathbb{Z} of the integers, with conventional addition and multiplication, is a unitary ring called the ring of integers.

A ring that has a neutral element for the multiplication (called a unity) is called a unitary ring or a ring, depending on the authors.

A.2 Ideals

Let A be a ring, and B a nonempty subset of A . B is a subring of A if, and only if, B is closed with respect to subtraction and multiplication. It exists a special subrings called ideals which are the counterpart of normal subgroups.

A nonempty subset B of a ring A is called ideal of A if B is closed with respect to addition and negatives, and B absorbs products in A .

A simple example of an ideal is the set \mathbb{E} of the even integers. \mathbb{E} is an ideal of \mathbb{Z} because the sum of two even integers is even, the negative of any even integer is even, and, finally, the product of an even integer with an integer is always even.

A.3 Rings of Polynomials

Suppose we wish to enlarge the ring \mathbb{Z} by adding to it the number π . It is easy to see that we will have to adjoin to \mathbb{Z} other new numbers besides just π ; for the enlarged ring will also contain such things as $-\pi, \pi + 7, 6\pi^2 - 11$, and so on. As a matter of fact, any ring which contains \mathbb{Z} as a subring and which also contains the number π will have to contain every number of the form:

$$a\pi^n + b\pi^{n-1} + \dots + k\pi + l \tag{A.3}$$

where a, b, \dots, k, l are integers. In other words, it will contain all the polynomial expressions in π with integer coefficients.

But the set of all the polynomial expressions in π with integer coefficients is a ring. This ring contains \mathbb{Z} because every integer a is a polynomial with a constant term only,

and it also contains π .

In elementary algebra, one considers polynomials whose coefficients are real numbers, or in some cases, complex numbers. As a matter of fact, the properties of polynomials are independent of the exact nature of the coefficients. All we need to know is that the coefficients are contained in a ring. This ring is assumed to be commutative with unity.

Let A be a commutative ring with unitary, and x in arbitrary symbol. Every expression of the form

$$a_0 + a_1x + a_2x^2 + \dots + a_nx^n \quad (\text{A.4})$$

is called a polynomial in x over A

A.4 Division Algorithm for Polynomials

If $a(x)$ and $b(x)$ are polynomials over a field F , and $b(x) \neq 0$, there exists polynomials $q(x)$ and $r(x)$ over F such that

$$a(x) = b(x)q(x) + r(x) \quad (\text{A.5})$$

and

$$r(x) = 0 \quad \text{or} \quad \deg r(x) < \deg b(x) \quad (\text{A.6})$$

A.5 Wu's Method

This section is based on the Book called Ideals, Varieties, and Algorithms from David Cox. More detailed information could be find in [33].

The idea here is to follow the one-variable polynomial division algorithm as closely as possible, and we obtain a result known as the pseudo-division algorithm.

Let $f, g \in K[x_1, \dots, x_n, y]$ be as:

$$\begin{aligned} f &= c_p y^p + \dots + c_1 y + c_0. \\ g &= d_m y^m + \dots + d_1 y + d_0. \end{aligned} \tag{A.7}$$

Assume $m \leq p$ and $g \neq 0$. There is an equation

$$d_m^s f = qg + r, \tag{A.8}$$

where $q, r \in K[x_1, \dots, x_n, y]$, $s \geq 0$, and either $r = 0$ or the degree of r in y is less than m . Also $r \in \langle f, g \rangle$ in the ring $K[x_1, \dots, x_n, y]$.

Wu's method uses pseudo-division to reduce the hypotheses expressed as polynomials whose set of common zeroes is denoted as V to a system of polynomials f_j that are in triangular form in the variables x_1, \dots, x_n . Then, it uses successive pseudo-division of the conclusion g with respect to each one of the polynomials f_j to determine whether g is in the ideal generated by the f_j , thus in $I(V)$.